Review of Cellulose Smart Material: Biomass Conversion Process and Progress on Cellulose-Based Electroactive Paper

S.H. Hassan[1,2], Lee Hwei Voon[1]*, T.S. Velayutham[2]*, Lindong Zhai[3], Hyun Chan Kim[3] and Jaehwan Kim[3]

[1]*Nanotechnology and Catalysis Research Center (NanoCat), Institute of Postgraduate Studies, University of Malaya, 50603 Kuala Lumpur, Malaysia*
[2]*Low Dimensional Materials Research Center, Department of Physics, Faculty of Science, University of Malaya, 50603 Kuala Lumpur, Malaysia*
[3]*Department of Mechanical Engineering, Inha University, Incheon 22212, South Korea*

Received June 15, 2017; Accepted September 22, 2017

ABSTRACT Cellulose is a renewable biomass material and natural polymer which is abundantly available on Earth, and includes agricultural wastes, forestry residues, and woody materials. The excellent and smart characteristics of cellulose materials, such as lightweight, biocompatibility, biodegradability, high mechanical strength/stiffness and low thermal expansibility, have made cellulose a high-potential material for various industry applications. Cellulose has recently been discovered as a smart material in the electroactive polymers family which carries the name of cellulose-based electroactive paper (EAPap). The shear piezoelectricity in cellulose polymers is able to induce large displacement output, low actuation voltage, and low power consumption in the application of biomimetic sensors/actuators and electromechanical system. The present study provides an overview of biomass pretreatment from various lignocellulosic cellulose (LC) resources and nanocellulose production via TEMPO-mediated oxidation reaction, followed by the production of different types of EAPap versus its performance, and lastly the applications of EAPap in different areas and industries. Specifically, LC biomass consists mainly of cellulose having a small content of hemicelluloses and lignins which form a defensive inner structure against the degradation of plant cell wall. Thus, selective approaches are discussed to ensure proper extraction of cellulosic fibers from complex biomass for further minimization to nano-dimensions. In addition, a comprehensive review of the development of cellulose-based EAPap as well as fabrication, characterization, performance enhancement and applications of EAPap devices are discussed herein.

KEYWORDS: Biomass pretreatment, nanocellulose, renewable materials, smart materials, actuators

1 INTRODUCTION

The drastic growth of global energy consumption, depletion of fossil fuel reserves as well as climate change have created a high demand for renewable materials which are less harmful to the environment in order to ensure the sustainability of our society and environment [1, 2]. The burning of fossil fuels has led to severe environmental problems such as the emission of greenhouse gases and air pollutants. In contrast, the use of renewable materials has been proven as a way to produce zero emissions [3, 4], which could reduce the negative impact on the environment [5]. For the past several years, researchers have been focusing on lignocellulosic cellulose (LC), which is a renewable polymer, for various methods of alternative petrochemical production [3, 6]. The LC biomass is derived from different sources such as agricultural residues, forestry residues and energy crops [7, 8].

Typically, the main composition of LC biomass is cellulose, hemicelluloses and lignins, which are bundled in a complex structure of cell walls [9–11]. The chemical composition might vary for different species

**Corresponding author*: leehweivoon@um.edu.my; t_selvi@um.edu.my

DOI: 10.7569/JRM.2017.634173

Table 1 Chemical composition of lignocellulose in different resources [3, 8, 9, 12].

Lignocellulosic resources	Cellulose (%)	Hemicellulose (%)	Lignin (%)
Agriculture residues			
Nut shells	25–30	25–30	30–40
Corn stalks	48	29	16
Corn cobs	45	35	15
Sugar cane bagasse	42	25	20
Wheat straw	30	50	15
Rice straw	32.1	24	18
Coffee pulp	35	46.3	18
Forest residue			
Hardwoods stems	40–55	24–40	18–25
Softwood stems	45–50	25–35	25–35
Energy crop			
Grasses	25–40	35–50	10–30
Coastal Bermuda grass	25	35.7	6.4
Switch grass	45	31.4	12.0

of plants (Table 1) [3, 8, 9, 12]. Cellulose is the major constituent among the other components which support the structural components of the cell walls [3, 9]. It has many prominent properties such as high modulus and tensile strength, excellent mechanical strength, hydrophilicity, biocompatibility, biodegradability and relative thermal-stability [13, 14]. This study reviews the latest advancements in cellulose and nanocellulose technologies which consist of the preparation, properties and applications of cellulose and nanocellulose, possible application as EAPap, followed by highlights of methodologies and readiness of EAPap. The development of EAPap is extensively elaborated, including the fabrication, characterization and its applications such as piezoelectric EAPap, flying magic paper and biodegradable microelectromechanical systems (MEMS).

1.1 Cellulose and Nanocellulose Chemistry

Cellulose is the most abundant source of raw materials with worldwide production of approximately 1.5×10^{12} tons per year [15, 16]. The agricultural and forestry residues are the highest contributors to this cellulose annual production. However, only less than 2% of the cellulose is recovered industrially by various applications in the furniture industry, paper production, textile production, biocomposites, chemical industry and pharmaceutical industry, among others. Cellulose is a long-chain polysaccharide made up of D-glucose ($(C_6H_{10}O_5)_n$) which is connected by β-1-4-linkages [17]. Every monomer consists of three hydroxyl groups which have the ability to form hydrogen bonds to support cellulose with a highly ordered three-dimensional crystal structure [10, 18]. In addition, the molecular aggregation of cellulose in plant cell wall contributes to its unique polymer properties. This phenomenon occurs primarily via intra- and intermolecular hydrogen bonds between the cellulose chains, which lead to parallel arrangement of cellulose chains organized in a sheet-like structure. Cellulose fibers are stabilized by interchain OH–O hydrogen bonds to form flat chain sheets with weak CH–O hydrogen bonds between the fibrils [19]. These good inherent properties of cellulose and low production cost have enabled it to be applied in many areas [20].

Nanocellulose is generally referred to as a cellulose particle having at least one dimension in the nanometer range (1–100 nm) [21, 22]. Nanocellulose exhibits numerous remarkable properties such as high mechanical strength, extensive surface area, unique optical properties, high crystallinity and stiffness [7, 18]. There are three types of nanocellulose (refer to Figure 1), i.e., (i) microfibrillated cellulose (MFC) or nanofibrillated cellulose (NFC), (ii) nanocrystalline cellulose (NCC) or cellulose nanocrystal (CNC) and (iii) bacterial cellulose (BC). Nanocellulose either in longer cellulose nanofibrils (CNFs) or rod-like CNCs is known by a variety of names such as nanocrystals, rods, whiskers, nanofibers or nanofibrils [19, 23]. The aspect ratios of NCC are much lower than MFC due to the presence of amorphous regions in the microfibrils. In contrast, the stiffness and modulus of NCC with more crystalline regions are higher than those of MFC and BC fibrils with both crystalline and amorphous structures [24].

1.2 Conversion of Biomass via TEMPO-Mediated Oxidation

The diversity of cellulose and nanocellulose particles is highly dependent on its source and extraction process. Therefore, the choice of biomass pretreatment is a key element of the biomass conversion process [25]. Since LC biomass is mainly composed of cellulose, hemicelluloses and lignins, it is mandatory for cellulose fibers to undergo a biomass pretreatment process in order to separate each constituent's fiber components which are connected in the cell wall structure [26]. According to Harmsen *et al.*, the pretreatment process contributes to several advantages such as increased surface area and porosity of cellulose and it is also a cost-effective technique to further depolymerize the cellulose into other biochemicals [27].

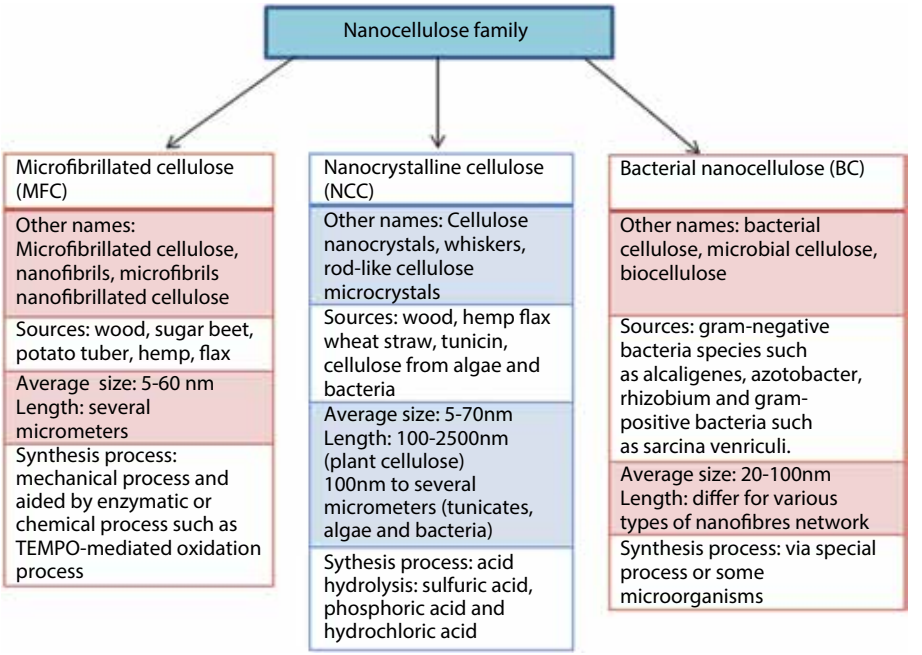

Figure 1 The family of nanocellulose materials [28, 29].

The removal of highly complex lignins is an essential processing step during the extraction of cellulose fibers because the lignins are crosslinked polymers that act to bind the cellulose fibers, which disrupt the extraction process of cellulose [28]. The elimination of lignins increases the effectiveness of the pretreatment process as the acids or enzymes can easily access and act on the cellulose chains, subsequently hydrolyzing the cellulose. There are several types of pretreatments, i.e., physical (milling and grinding), chemical (alkaline, oxidizing agents, dilute acid and organic solvents), biological and multiple or a combination of physical and chemical pretreatments (steam pretreatment/autohydrolysis, hydrothermolysis and wet oxidation) [8, 11, 29]. Specifically, bleaching or cellulose purification is aimed at accurately removing the lignins with the production of a homogeneous final product [25]. In most cases, alkaline pretreatment using hydrogen peroxide was used, as it is one of the most efficient and eco-friendly bleaching pathways [30]. Most of the pretreatment processes suffered unsatisfactory separation of celluloses and lignins due to over-degradation, which has led to the formation of by-products such as sugar rather than nanocellulose. Therefore, a suitable biomass pretreatment technology with mild reaction conditions and effective cellulose recovery is highly appreciated in order to reduce utility consumption, lower power usage, reduce capital cost, and reduce cellulose degradation to sugar by-product [31].

Generally, the chemical process is the most popular technology in the isolation of cellulose fibers from biomass due to its high efficiency and lower treatment cost [29, 31]. Various chemical methods have been developed to extract the cellulose nanomaterial, i.e., acid hydrolysis [32–34], dilute acid [35, 36], mechanical defibrillation [37], organosolv [38, 39] and 2,2,6,6-tetramethylpiperidine-1-oxyl (TEMPO)-mediated oxidation [40–42]. At present, the most renowned technique for the extraction of cellulose nanomaterial is TEMPO-mediated oxidation because it permits the preparation of cellulose nanofibrils with high aspect ratio. Addition of NaClO (the primary oxidant) solution with the presence of catalyst NaBr and TEMPO lead to the oxidation of cellulose fibers [43, 44]. The reaction was favored in the pH range of 10–11 to ensure that the C6 primary hydroxyls of cellulose were oxidized to C6 carboxylate groups [44, 45]. The oxidized products are almost homogeneous with a chemical structure of Na(1→4)-β-D-poly-glucuronate or Na salt of celluoronic acid (CUA) which consisted of D-glucuronosyl units alone [40].

In recent studies, stable nitroxyl radicals were utilized for the catalytic oxidation (e.g., TEMPO) in order to prepare cellulose nanomaterial under mild reaction condition [46]. In most reactions, hypochlorite (ClO^-) was used as essential oxidant and bromide (Br^-) was used as a co-catalyst [46]. A general reaction scheme of oxidation using the TEMPO system is depicted in refs. [40, 44, 46].

Jiang and Hsieh reported the extraction of CNC and CNFs from pure rice straw using three types of pretreatments: (i) sulfuric acid hydrolysis; (ii)

mechanical blending; and (iii) TEMPO-mediated oxidation, to differentiate the morphologies and surface properties of the nanocellulose products from each treatment [23]. Results indicated that CNFs prepared by TEMPO-mediated oxidation demonstrated the finest fibril (1.7 nm) of nanocellulose with the highest uniformity in width, and the highest yield (19.7%) as compared to other methods [23]. During TEMPO-mediated oxidation, the hydroxyl group of cellulose was converted to surface C6 carboxyls via oxidation process. Thus, the presence of both carbonyl and hydroxyl double dipoles of the TEMPO-mediated oxidized cellulose nanofibril (TOCN) rendered higher hydrogen bonding capabilities. In addition, the presence of carbonyl and hydroxyl double dipoles created a charge repellent environment, which individualized the fibrils into smaller widths and uniform lateral dimensions of fibers with higher surface area [23].

In another study, Saito *et al.* [44] used TEMPO-mediated oxidation to individualize the hardwood bleached kraft pulp through direct surface carboxylation. The carboxylate of the oxidized cellulose fibers was disintegrated in water and it was highly crystalline with individual fibrils (approximately 5 nm in width and 2 µm long). The oxidized cellulose had a high degree of polymerization (> 900) with absence of aldehyde group due to the oxidation of aldehyde into carboxyl group during the oxidation process [44]. The oxidized cellulose fibrils (nanocellulose fibrils with high aspect ratio) were cast into films using the water dispersion method. The cast films were transparent, flexible and showed high elasticity of 312 MPa with a low density of 1.47g/cm^3 [44].

Tanaka *et al.* [47] prepared cellulose nanofibrils from softwood bleached kraft pulps by using $NaClO_2$ (primary oxidant), and 2,2,6,6-tetramethylpiperidine-1-oxyl (4-H-TEMPO) or 4-Acetamido-TEMPO (4-AcNH-TEMPO) in aqueous buffer under pH 4.8 or 6.8. The 4-AcNH-TEMPO-oxidized cellulose was converted to individual nanofibrils in the presence of mechanical disintegration under water. The carboxylate content of TEMPO-mediated oxidized CNFs was 1.3 mmol/g [47].

Fukuzumi [48] used raw wood chips for the pulping process. Pulping reagents were used in the mechanical and chemical processes so that the lignins were removed from the wood chips. The TOCN films consist of randomly assembled nanofibrils. The TOCNs from the softwood cellulose were flexible, transparent, highly rigid, exhibited high oxygen barrier properties and low coefficient of thermal expansion due to the high crystallinity of native cellulose [48]. Thus, the TOCN films possessed supermolecular characteristics which can be utilized in various applications, e.g., adaptable display panels, biomass-source packaging, electronic gadgets and many more.

Shinoda *et al.* [49] used softwood bleached kraft pulp to prepare TOCN via TEMPO-mediated oxidation and mechanical fibrillation treatments. The mechanical disintegration of oxidized cellulose in the water showed significant impact on the degree of polymerization for nanofibrils with apparent nanolength of products (measured as viscosity measurements: DPv). The DPv values were reduced from 1270 to 500–600 with the rise of NaClO content in the TEMPO-mediated oxidation stage. In addition, DPv values were further lowered when followed by mechanical fibrillation in water. The same case was similar with Jiang *et al.* [50], where coupling TEMPO-mediated oxidation with mechanical blending technique was used to prepare nanocellulose from rice straw. The strong defibrillation process has offered a versatile alternative to create superfine fibers with highly crystalline cellulose Iβ structure.

Dai *et al.* [51] found that TEMPO-mediated oxidation with the addition of formic corrosive pretreatment rendered efficient pathways to prepare cellulose nanofibrils from bleached softwood kraft pulp with the aid of mechanical homogenizer. The presence of formic acid was able to induce the oxidation of native cellulose for the fibrillation process to nanocellulose. The results showed that the ideal concentration of formic acid was 5% (v/v) and the highest carboxyl content of oxidized cellulose was 1.769 mmol/g [51].

Bettaieb's group [52] reported the extraction of different grades of CNF from *Posidonia oceanica* (*P. oceanica*) balls and leaves using TEMPO-mediated oxidation process with various concentrations of oxidants. The suspensions produced from the process were further disintegrated using "Masuko's Supermasscolloider" ultra-fine friction grinder. The higher concentration of oxidant rendered stronger fibrous network structures with an increase of the storage modulus.

Oun and Rhim [53] successfully extracted cellulose nanocrystals (CNCs) and cellulose nanofibers (CNFs) from seed fibers of *Calotropis procera* (Ushar). The seed fiber of Ushar was processed using acid hydrolysis and TEMPO-mediated oxidation methods, respectively. The CNCs produced were needle shape with the yield of 79% with diameter of 14–24 nm and a length of approximately 140–260 nm. The CNF showed a web-like long fibrous structure with the higher yield at 98%, with diameter of around 10–20 nm and length in the micro-range [53]. The crystallinity of CNC and CNF were 70% and 59%, and the onset temperatures for the thermal decomposition were 240 °C and 200 °C, respectively. Thus, isolated CNCs and CNFs derived

from the Ushar seed fiber have potential to be made into reinforced biopolymer films for many applications, e.g., tissue designing, biomedical paper, food packaging, textiles, and many more. In addition, Miao *et al.* [54] have successfully extracted CNFs from cotton stalk bark using a similar process, i.e., a combination of TEMPO-mediated oxygen and mechanical disintegration methods.

In another study, Meng *et al.* [55] used four different types of fiber sources: fully bleached kraft pulp of softwood (pine) and hardwoods (eucalyptus) and non-woods (bamboo and bagasse) to examine the general role of non-cellulosic heteropolysaccharides (polymers of hemicellulose: galactoglucomannan, xylan, mannose, arabinose, galactose) during the production of TEMPO-oxidized cellulose nanofibers (TOCNs). Four types of sources were subjected to TEMPO-mediated oxidation with the aid of high-pressure homogenization for the production of TOCNs. Results indicated that most of the galactoglucomannan were removed during the oxidation process while the majority of xylans were retained due to the absence of C6 primary hydroxyl group [55]. Thus, the retained xylan will affect the formation of carboxylate group on the cellulose surface during the oxidation step by limiting the chemicals (TEMPO oxidopant, NaClO) available to cellulose. On the other hand, the lower content of xylan rendered transparency characteristic and eased the process of suspensions. Thus, the heteropolysaccharides structural process assisted by the mechanical method was able to enhance the nanofibrillation of cellulose fibers. The results showed that the final average widths were ~ 4 nm and average lengths of TOCNs of each source were 290, 350, 360 and 370 nm for eucalyptus, bamboo, bagasse, and pine, respectively. Based on the study, the carboxylate groups on cellulose surface via TEMPO-oxidation for pine, eucalyptus, bamboo, and bagasse were 0.89, 0.91, 0.87, and 0.82 mmol/g o.d.p [55], respectively. Thus, the study summarized that a lower level of heteropolysaccharides in TOCNs rendered different characteristics in terms of transparency and viscosity of the product.

Moreover, the presence of hemicellulose (xylans and galactoglucomannan) during the oxidation process limited the formation of carboxylate groups, which hindered the chemical accessibility to the cellulose structure [56]. The biomass pretreatment is an important step to solubilize the non-cellulosic content and isolate the native celluloses into nanofibers via surface modification, while maintaining the fibrous morphology and increasing the crystallinity of the nanofibers [56, 57]. Thus, utilization of TEMPO for the catalytic oxidation of cellulose fibers has generated an effective chemistry conversion of hydroxyl groups to aldehydes and carboxyl groups under mild conditions. Numerous related studies have recently been done and are reviewed in Table 2.

2 APPLICATION OF CELLULOSE AND NANOCELLULOSE AS SMART MATERIAL

Cellulose itself has limited functionalities in its original form. Nevertheless, the hierarchical structures produced by cellulose fibers at different length scale, combined with the ability to adopt other functional materials, have opened up many opportunities for high-end products. For instance, the nanofiber cellulose composites were used in the making of flexible circuits [58–60], solar panels [60] and electronic devices [61, 62]. Meanwhile, in the medical field, nanocellulose was used as implant material (artificial organs) [62, 63], biodegradable tissue scaffold [64] and drug delivery vehicle [24, 65, 66].

Lately, nanocellulose-based electroactive paper (EAPap) has attracted much attention as a smart material [57, 67–71]. Utilization of EAPap for flexible energy storage and electronic devices has taken cellulose technology to another level compared to commercial paper with rough surface and weak mechanical properties [14, 72]. In addition, preparation of nanocellulose-based smart material via chemical modification and physical incorporation or blending in various forms affects the physicochemical properties of the products, i.e., responsiveness to pH, temperature, light, mechanical forces, electricity, and magnetic field. The presence of porosity and refractive index variation has made EAPap a feature with extraordinary light-scattering effect (used as a transparent paper) for use in integrated transparent sensors and 3D microfluidic application. Furthermore, nanocellulose-based EAPap portrayed several superior characteristics such as ultra-lightweight, large bending deformation, low actuation voltage and low power consumption. These characteristics are very appealing for delicate biomimetic actuators, dynamic wings for flying articles, active sound-absorbing materials, adaptable speakers and smart shape control gadgets [70, 73, 74]. The following sections are dedicated to cellulose-based EAPap where a complete review of preparation, actuation principle, characterization, current progress in improving the performance of EAPap and the possible applications are discussed.

2.1 Electroactive Paper (EAPap)

The EAPap actuator is a chemically treated paper with thin electrodes on both sides. Figure 2 shows a

Table 2 The detailed pretreatment of lignocellulosic biomass via TEMPO-oxidations.

Chemical treatment							
Biomass	**Synthesis**	**Concentration of chemicals**	**Reaction time**	**Temperature**	**Dimension / aspect ratio (L/d)**	**Crystallinity**	**Reference**
Pure rice straw	TEMPO-mediated oxidation	0.016 g	65 min	N/A	(1.7 nm) and micrometer long	64.4% CrI	[23]
hardwood kraft pulp	TEMPO-mediated Oxidation	0.016 g	2–72 h	60 °C	5nm in width and at least 2µm in length	N/A	[44]
Kraft pulps	TEMPO-mediated Oxidation	0.10 g	48 h	40 ºC	3–4 nm and lengths greater than 1µm.	69 % CrI	[47]
Softwood kraft pulp fibers	TEMPO-mediated Oxidation	0.016 g	N/A	25 ºC	3-4nm	75 % CrI	[48]
Softwood kraft pulp	TEMPO-mediated Oxidation	0.08 g	0.5 h	25 ºC	~1 µm to ~500 nm	N/A	[49]
rice straw	TEMPO-mediated Oxidation	0.016 g	50 min	25 ºC	125–497 nm wide	63.2–71.5% CrI	[50]
Softwood kraft pulp	TEMPO-mediated Oxidation	0.10 g	6 h	25 ºC	3–7 nm in width and 300–400 nm in length	N/A	[51]
Posidonia Oceanica balls and leaves	TEMPO-mediated Oxidation	0.10 g	2 h	25 ºC	Posidonia Oceanica balls: 5 to 21 nm Posidonia Oceanica leaves :2 to 15 nm	D/A	[52]
Ushar (Calotropis Procera) seed fibers	TEMPO-mediated oxidation	1.0 g	N/A	25 ºC	CNF : diameter of 10–20 nm	59 % CrI	[53]
pristine cotton stalk barks	TEMPO-oxidation and mechanical disintegration methods	0.033 g	2.5 h	N/A	A length of several micrometers and a width in 5-10nm	72.5% CrI	[54]
Pine Eucalyptus Bamboo Bagasse	TEMPO-mediated Oxidation	0.015 g	N/A	25 ºC	average length: 290 nm 350 nm 360 nm 370 nm, with average widths of ~4 nm	75.9% 69.1% 71.5% 68.7%	[55]

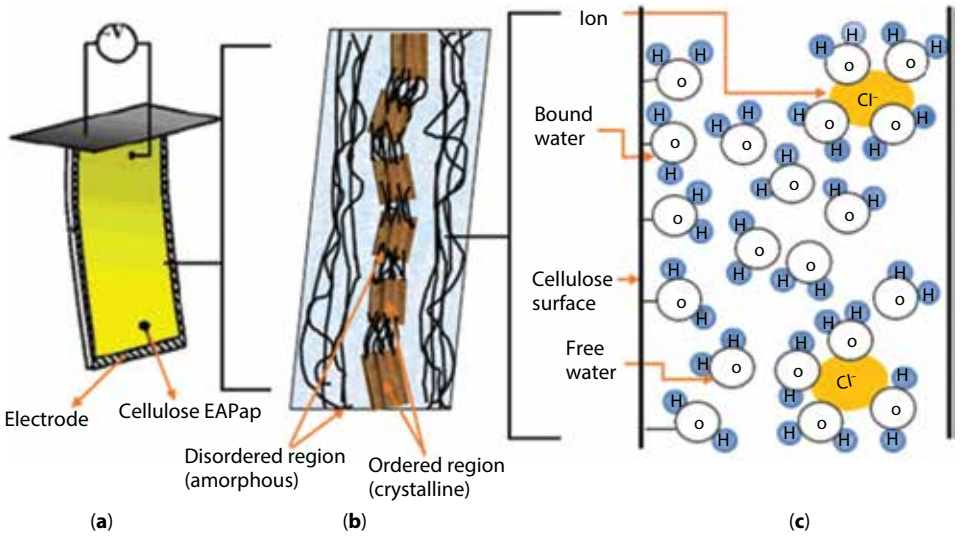

Figure 2 Schematic diagram of (**a**) EAPap where gold electrodes are deposited on both sides; (**b**) cellulose microfibril with ordered crystalline regions and disordered regions; (**c**) the water molecules which are bonded with hydroxyls on the cellulose surface (bound water) or clustered freely in the microfibril (free water) [75].

schematic diagram of an electroactive paper [75]. The research on EAPap was initiated by Kim and Seo in the year 2000 [71]. Various kinds of fibrous papers from softwood, hardwood, cellophane, bacterial cellulose, Kraft paper, electrolyte paper, Korean paper, and carbon paper were selected in the research to study and examine the electroactive characteristics of the papers [71]. The performance of the EAPap is dependent on many factors such as electrodes, alignment of cellulose films, environmental conditions, solvents, the thicknesses and the electrode patterns on the films. In order to fully understand the many factors that influence the performance of the EAPap, it is essential to understand the actuation principle of the cellulose.

2.2 Actuation Principle of EAPap

The electroactive behavior of EAPap is due to its unique crystalline structure and piezoelectric behavior of the cellulose [76]. The actuation phenomenon is based on three combined effects: piezoelectricity, ionic migration and a non-uniform spatial dielectric constant due to water absorption [77–82]. The cellulose II crystal is monoclinic and non-centrosymmetric in nature and thus it exhibits piezoelectric characteristics [68, 79, 83]. The piezoelectricity is due to the disordered regions where the dipoles are stabilized into permanent polarization [68, 78, 83]. The permanent dipoles in cellulose were the hydroxyl and carboxyl groups in its molecular structure. Water molecules were attached to the hydroxyl groups in the large disordered cellulose chain [79]. The existence of disordered regions increased the localized states that linked with the hydrogen bond of cellulose chains [73, 83] and the charge transfer process dominated in these localized states. Both combinations of piezoelectricity and migration effects of the charge carriers in the cellulose have contributed to the actuation of the EAPap.

3 ELECTROACTIVE PAPER FABRICATION TECHNIQUE

The efficiency of the EAPap can be enhanced thru a controlled fabrication technique. Figure 3 summarizes the fabrication process of the EAPap [84]. The process involves many stages and cycles [85–87]. The first step is to dissolve cellulose pulp or cotton using lithium chloride and N,N-dimethylacetamide (DMAc) solvent. Kim *et al.* [75] used cotton pulp (natural cellulose) with a degree of polymerization (DP) of approximately 4500. The cellulose can be regenerated using many different methods [88], while the preparation of EAPap using natural cellulose involved special solvents. The regenerating process improved the crystallinity and the alignment of the fibers. Preparation of the EAPap started with drying of cotton pulp in an oven at 100 °C. The dried cotton was then dissolved by mechanical stirring at 155 °C using a mixture of solvents, i.e., lithium chloride (LiCl) and anhydrous N,N-dimethylacetamide (DMAc). During the process, the proportion of mixture (cotton/LiCl/DMAc) switched between two ratios; 2/8/90 [75, 87, 89–93] and 1.5/8.5/90 [94]. The non-dissolved cellulose

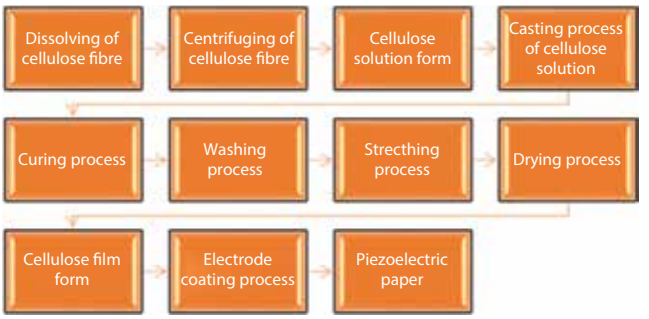

Figure 3 The fabrication process of EAPap [84].

fibers were eliminated through centrifugation at 1100 rpm and the clear cellulose solution was casted on a glass plate using a doctor blade to obtain a film with uniform thickness. The films were cured by immersing them in a mixture of deionized (DI) water and isopropyl alcohol (DI/IPA) bath for 24 h to effectively remove the Li^+ (DMAc) macro-cations from the cellulose matrix. Mechanical stretching was applied on the wet or dried cellulose film with a drawing ratio (DR: used to compare the ratio between the stretched length of the film with the orginal length) of approximately 1.5–2 in order to increase the alignment of the cellulose chains in the in-plane directions [89]. The stretched film was dried under an infrared ray heater for about one hour and subsequently thin electrodes were deposited onto both sides of the film using physical vapor deposition [95] or thermal vapor deposition techniques [77, 85, 96].

Recently, Zhai *et al.* [92] reported a better fabrication technique of EAPap by facile solvent exchange pretreatment using cotton pulp. The pretreatment of cellulose with exchange facile solvent showed the highest piezoelectric charge constant and it was proven to be more convenient and efficient than the previous suggested techniques.

3.1 EAPap Characterization

The characterization of EAPap is crucial to understand and improve its electroactive characteristics so that it can be employed and utilized precisely in numerous applications. In order to understand the detailed properties of EAPap, the mechanical and electrical properties were studied by obtaining the induced strain, blocked force, piezoelectricity, aligning effects, strength, stiffness and creep behavior of the EAPap [73, 79, 97–99]. These characteristics were explored and studied in terms of mechanical, electrical and physical tests. The mechanical strain and strength were examined by sheet level and thermomechanical analysis. Meanwhile, the electrical resistance and admittance were analyzed to investigate the actuation mechanism. EAPap which met a certain standard of force and displacement tests will be pertinent to various applications, e.g., instant wings for flying objects, active sound-absorbing materials, flexible speakers and smart shape control devices [76]. The aim of the following section is to provide an overview of the methods available for the investigation of electroactive characteristics of EAPap.

3.1.1 *Direct Piezoelectricity*

Direct piezoelectricity, which is the key mechanism in the EAPap, was measured by mechanically stretching the piezoelectric material. Piezoelectricity in a monoclinic cellulose was first reported by Fukada in 1950 [100, 101]. The uniaxially oriented system of cellulose crystallites exhibits shear piezoelectricity in which the piezoelectric constants $d_{14} = d_{25}$ are finite and the other components are zero. Studies has shown a noteworthy piezoelectric constant which was strongly dependent on the material orientation of EAPap and the alignment of disordered regions of cellulose [102]. A previous study has shown that the d_{25} of regenerated nanocrystalline cellulose II was measured in the range of 35 to 60 pC/N [103]. The piezoelectric property of the EAPap as a function of material alignment of the cellulose paper was studied [89, 98]. Three different material orientations classified as 0°, 45° and 90° were studied, as shown in Figure 4 [98, 99]. Elastic stiffness and strength of EAPap were strongly dependent on the orientation of the material. A large relative increment of mechanical properties was observed in the 45° oriented sample under the electric excitation with the measured piezoelectric charge constant of approximately 28 pC/N. This was simply due to the shear piezoelectric nature of the cellulose film.

Direct piezoelectricity was investigated by determining the induced charge and the induced voltage under in-plane normal static/dynamic load [87]. Amidst the tensile test, the induced charge created from EAPap was measured by a picoammeter (Keithley 6485) [67]. The piezoelectric charge constant measurement setup for EAPap is schematically shown in Figure 5 [67, 89]. The electrical displacement and normal stress were used to determine the in-plane piezoelectric charge constant, d_{25} [92], using the following equation:

$$d_{25} = \left(\frac{\partial D}{\partial T}\right)_E \quad (1)$$

where is the induced charge per unit electrode area and is the applied in-plane normal stress. The induced charge was measured using the quasi-static method with no electric field applied during the tensile test.

Whilst stretching the EAPap, the induced charge on the electrode was measured and the piezoelectric

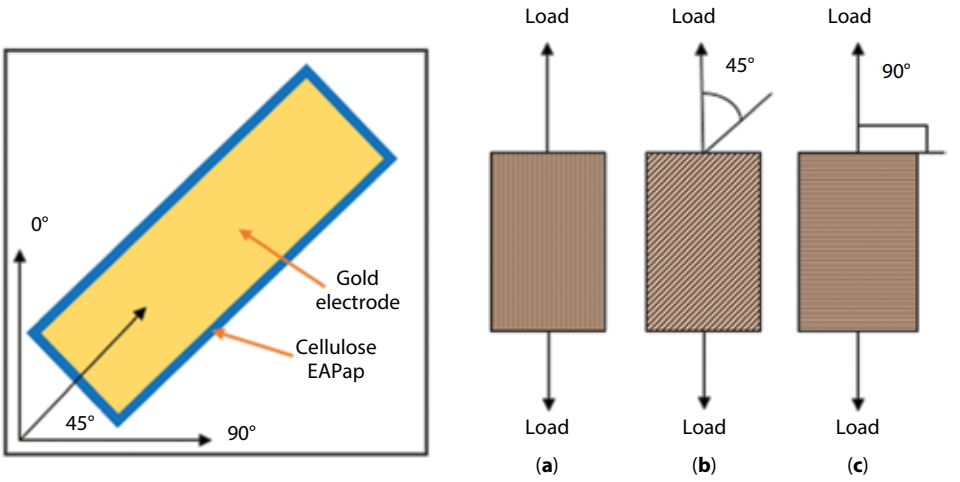

Figure 4 The configuration of the prepared EAPap samples and orientations of three different materials of EAPap: (**a**) 0°, (**b**) 45° and (**c**) 90° [98, 99].

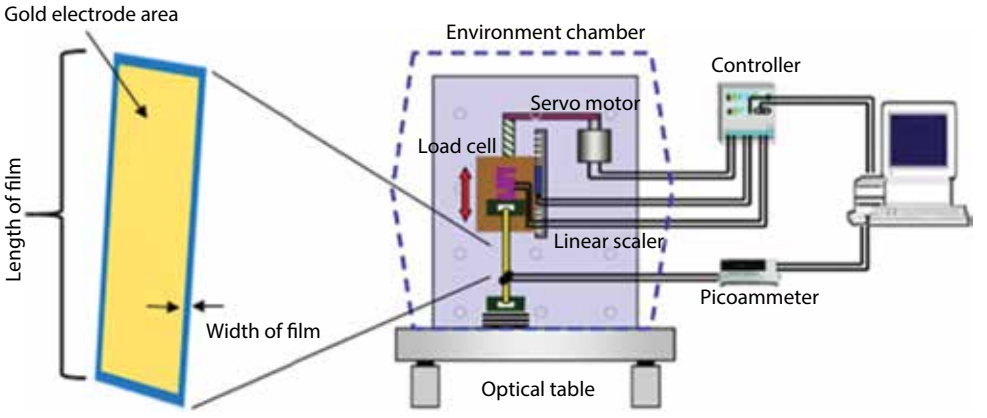

Figure 5 Schematic diagram of piezoelectric charge constant measurement setup [68, 89].

charge constant was calculated using Equation 1 [89, 104, 105]. The measured piezoelectric charge contstant with various alignments is shown in ref. [89]. Higher piezoelectric charge constant was observed for higher DR [104] and the 45° alignment of DR2.0 showed the highest piezoelectric charge constant, while the 90° alignment showed the same results as the piezoelectric charge constant of the non-stretched sample [89, 104].

3.1.2 *Mechanical Properties of EAPap*

EAPap is a complex anisotropic material with decreasing axial strength at moderate temperature and humid environment [106, 107]. The mechanical properties of EAPap were investigated using tensile tests to examine the dependence of stress and strain under various environmental conditions and configurations [108]. Mechanical test on EAPap was performed according to the ASTM D882-12 standard test method [79, 87, 106]. A typical stress-strain plot of the EAPap is depicted in Figure 6. The bifurcation point (σ_b,ε_b) was determined by the intersection point between the best fit straight line of the two curves, as shown in Figure 6

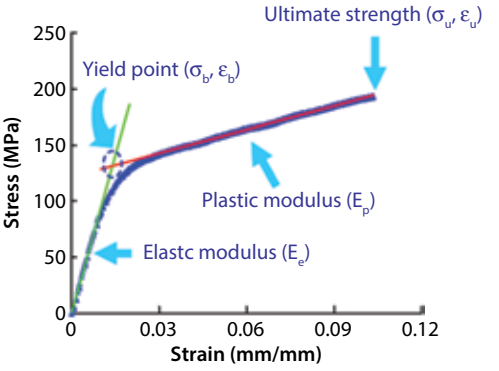

Figure 6 Tensile test results of cellophane [109].

[109]. The slopes of the graph were associated with the strength of cellulose nanofibrils (first curve) and the amorphous part (second curve) of the cellulose respectively [109]. The mechanical properties of the cellulose film with various temperatures, humidities, DRs and material orientations were reported in previous studies [79, 87, 110]. The elastic strength and stiffness were gradually decreased when the humidity and temperature were increased [79]. The dynamic test measured the creep behaviors of EAPap in constant stress and low-frequency cyclic stress [111].

Creep tests are performed to characterize the microscale deformations of EAPap [76]. Creep is a time-dependent inelastic material response to a constant load and is used to determine the deformation behavior of the film [76, 111]. The creep of EAPap was studied in the environment of the compounding temperature and humidity [76, 85, 110]. The experimental setup of the creep test in an environment chamber (Labcamp, CTHC-500P) is shown in Figure 7 [76]. The environmental chamber ensured constant temperature and humidity throughout the experiments.

The yield stress (σ_y) from the mechanical study is assumed as the reference of creep test conditions. In addition, the creep displacement as a function of time is measured using a laser displacement measurement sensor and the data is recorded by data acquisition system [76]. The time-dependent creep strain under different creep load conditions has been previously reported [76, 110]. The deformation phenomenon in the cellulose film is due to the breakage of inter-fiber bond or hydrogen bonds of the cellulose chains or molecules [110]. Microdimples or microcracks were observed in the films for the lower load conditions (lower than 10% of the yielding strength), which were not found in the films applied with higher load. The occurrence of microcrack was presumed to be a response due to the different mechanical properties in the cellulose. The cellulose film which contained only short and random fibers in amorphous region responded at lower loading conditions while the fibers in crystalline regions have sustained most of the creep loads to higher loading level [76, 110].

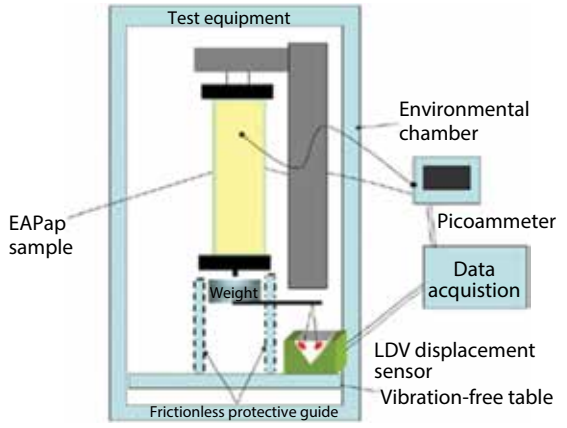

Figure 7 Schematic of the experimental setup for creep test [76].

3.1.3 *Electromechanical Properties of EAPap*

The electromechanical behavior of EAPap was identified by performing tensile tests under electrical excitation [89]. The experimental setup was similar to the piezoelectric measurement setup except for the picoammeter being replaced with a function generator. The function generator provides electrical excitation during the tensile test [98, 112].

The electromechanical coupling is obtained by comparing the elastic modulus, E_e, and ultimate strength, σ_u [73, 98]. The variations of E_e and σ_u of EAPap under different electric fields were reported in the literature [73, 98] in which both E_e, and σ_u increased with the increment of electric field and then started to decrease at higher electric field (~ 450 V/mm) due to the saturation phenomenon of elastic modulus and mechanical strength [85]. The electromechanical properties of EAPap at various degrees of alignment were investigated. The 45° oriented samples exhibited the largest relative increment of mechanical properties compared to 0° and 90° orientations [98].

3.1.4 *Morphology and Structure Determination of EAPap*

The structure and performance of EAPap were identified through various types of measurements. The morphology of the cellulose films was determined through scanning electron microscope (SEM) [75, 113–116]. The surface and cross-sectional images of soft and hardwood paper [71] and the morphology of the cellulose films were studied using SEM [92, 103]. The morphology of electrospun and spin-cast cellulose films were compared by Yun *et al.* [117]. The effect of solvent mixture on the properties and performance of the cured EAPap [118] and wet drawn cellulose were investigated using SEM [119]. The surface profile of the cellulose films was evaluated using atomic force microscopy (AFM) [118] and high voltage electron microscope (HVEM) [67]. The SEM, HVEM and AFM images of EAPap are shown in Figure 8 [67, 118].

The physical structure of the EAPap was determined using X-ray diffraction (XRD) and Fourier transform infrared spectroscopy (FTIR). XRD assisted in determining the crystalline structure of the cellulose film, while FTIR identified the presence of functional groups and impurities in the molecules. The possibility

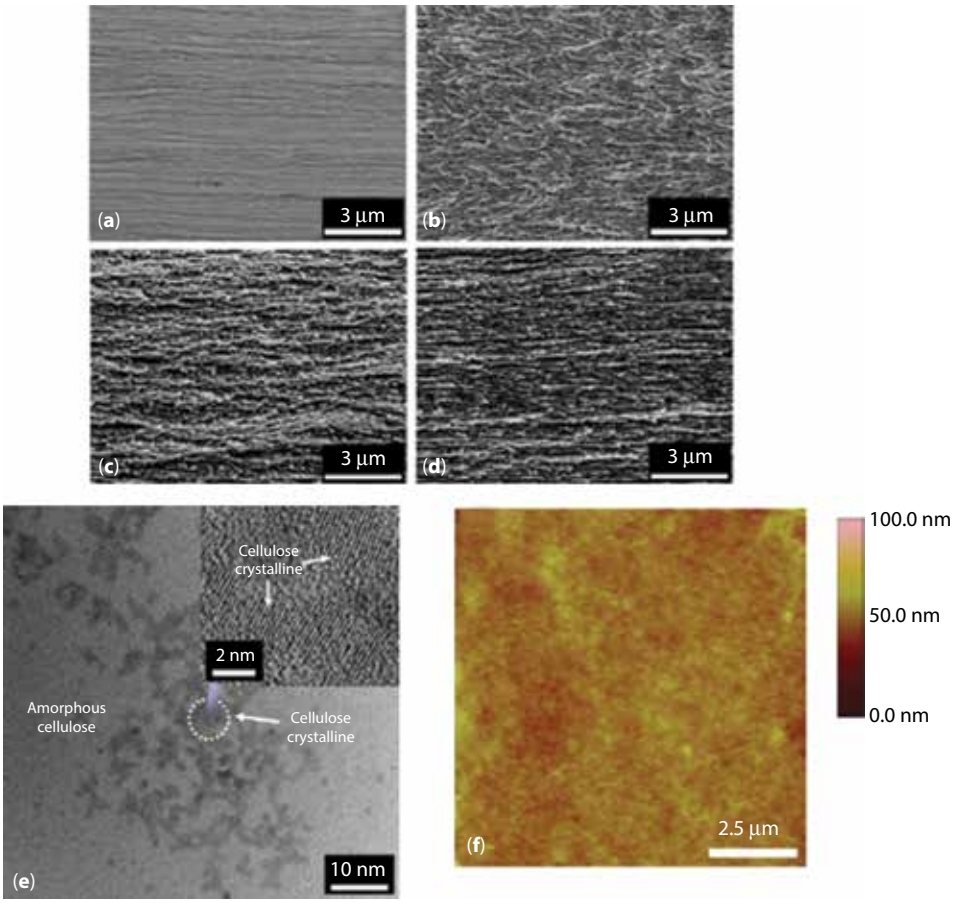

Figure 8 SEM cross-sectional images of cellulose films of various DRs, DR and electric field, *E*: (**a**) DR=1.0, *E*=0 V/mm, (**b**) DR=1.5, *E*=0 V/mm, (**c**) DR=1.5, *E*=20 V/mm, (**d**) DR=1.5, *E*=40 V/mm. (**e**) High voltage electron microscope image of nanofibers in regenerated cellulose prepared by applying E=40 V/mm and stretched with 50% strain [67]. (**f**) AFM image of cellulose film cured by DI:IPA, 40:60 solvent mixture [117].

of crystalline structure changes before and after the electrical activation was studied using XRD [120]. The structural changes related to the actuation behavior of cellulose were studied using XRD and FTIR results [107]. The FTIR spectra were analyzed between 700 to 3700 cm^{-1} wavenumber at various temperatures. The high intensity broadband around the wavenumber of 3300 cm^{-1}s was suggested as the stretching mode of O–H bond, while the intermediate bands at 1024 cm^{-1} corresponded to the C–O vibration of secondary alcohol and 1162 cm^{-1} was regarded as the stretching of C–O–C at β-(1~4)-glycosidic bond [107]. The FTIR peaks at 1334, 1427 and 1638 represented the bending position of C–O–C at C-2 or C-3, the bending of CH_2 and the primary amide from the DMAc [107], respectively. As the temperature increased (above 130°), the peak intensities decreased and most of the bands disappeared [107] due to the changes in the intra- and intermolecular hydrogen bonding and the packing of the cellulose molecules. The cellulose decomposed at ~240 °C. In another study, the XRD spectra of a regenerated cellulose has been reported [119] in which the peak intensity of (108) plane peak increased gradually with increasing DR from 1.0 to 2.0 [119]. However, after the actuation phenomenon, the (110) plane peak at 2θ = 12.26° decreases to 12.08°, while the (200) plane peak at 2θ = 21.64° increases slightly to 22.02°. These findings have suggested that structural changes related to crystallization of amorphous regions have occurred during the electrical actuation process [68].

Figure 8a–d shows the SEM images for the regenerated cellulose which are either stretched and/or applied different electric fields respectively. Figure 8a illustrates the non-stretched regenerated cellulose which shows a layered structure image. Figure 8b is the stretched regenerated cellulose (DR = 1.5) showing clusters of nanofibers in the cellulose matrix. The stretched films were applied with 20 V/mm and 40 V/mm electric field and the images are shown in Figure 8c and d, respectively. After the application of

electric field, the nanofibers structure was changed from cluster shape to a slender rod shape, with a uniform distribution throughout the cellulose matrix. On the other hand, Figure 8e shows the HVEM image of nanofibers of the regenerated cellulose. The crystalline cellulose chains are slightly darker compared to the amorphous cellulose matrix. The chain width (0.4300.036 nm) and the distance between two parallel chains (0.4740.042 nm) were obtained from the HVEM image. These images give evidence that both mechanical stretching and external electric fields enhance the configuration of nanofiber in regenerated cellulose and hence increase the crystallinity index of the sample. Figure 8f is the AFM image of the cellulose film which is normally used to sudy the surface profile of the film [118].

3.1.5 *Displacement Tests of EAPap*

The actuation phenomenon of EAPap was evaluated by measuring the bending displacement over time [118]. The measurement setup consisted of a function generator (Agilent, 33220A) and a high precision Laser Doppler vibrometer (LDV, Ometron VS100) mounted on an optical table and integrated with LabVIEW software for instrument control and data acquisition [121]. The function generator generated input AC voltage signal to the EAPap actuators and created a bending deformation, which is measured by the LDV. The LDV signals were then converted into displacement using LabVIEW software and analyzed. The LDV was not able to give information on the DC actuation displacement.

Blocked force measurement on the EAPap can give both the DC and AC actuation displacement. Figure 9 shows the schematic diagram of the blocked force measurement. Initial bending displacement was measured at the tip beam samples without any constraints and is referred to as free displacement. Meanwhile, the blocked force is the maximum force at the tip of the beam samples when the tip is fixed [97]. In a blocked force measurement setup, the tip was fixed, thus the tip displacement is zero and the force was set at the maximum (blocked force) [122]. Ideally, the blocked force is measured with zero displacements. However, it is very difficult to measure a very small blocked force, thus, a steel cantilever beam was introduced in the measurement setup (refer to Figure 9a,b). The bending stiffness of a cantilever beam is higher than that of the EAPap actuator. In this measurement, the tip displacement of the cantilever beam is measured when an electric field is applied to EAPap actuator and then is converted into force by using a point-loaded simple Euler-Bernoulli beam model. The typical force-displacement graph with the variation of actuation voltage for an EAPap is shown in Figure 9c. The area below the graph is the maximum mechanical work generated by the EAPap actuator [97]. As the actuation voltage increases, the displacement-force curve moves upward. Higher actuation voltage causes the actuator to have increased mechanical power.

A detailed explanation of the analysis has been reported in the literature [77, 97].

3.1.6 *Other Measurements*

The temperature and electric field effect of the EAPap was determined using thermally stimulated current (TSC) measurement [68, 96]. The dipole orientation in the cellulose film was identified by poling electric field and the corresponding depolarization current [68, 96]. The experimental setup for TSC measurement required a function generator (Agilent 33220A), a high voltage power amplifier (TREK PZD350 M/S)

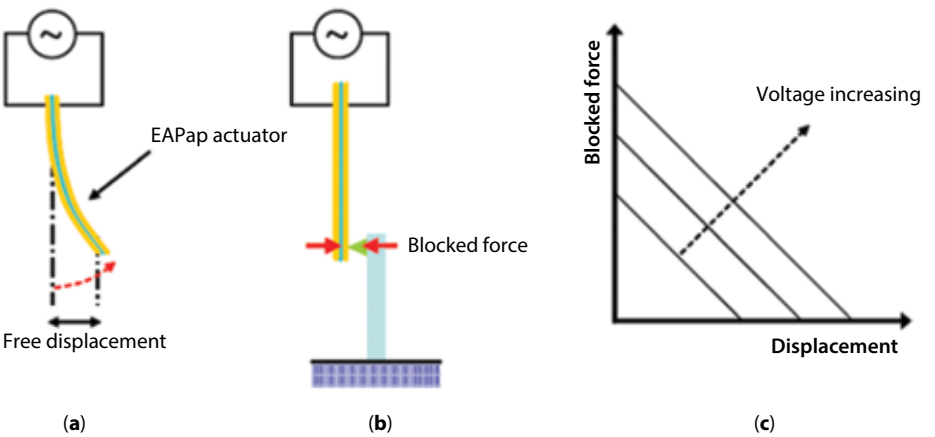

Figure 9 Schematic diagrams of performance parameters: (**a**) free displacement, (**b**) blocked force, (**c**) force-displacement relation with the variation of actuation voltage [97].

and a picoammeter (Keithley 6485) [96]. The depolarized current versus temperature of EAPap with different poling electric fields and the peak current values as a function of poling electric field were reported by Kim *et al*. [68]. The depolarization current increased linearly as the poling electric field increased and the results were related to the dipole orientation and piezoelectricity in the EAPap [68].

The dielectric constant of the cellulose is measured using impedance spectroscopy with varied frequency and temperature [71, 92, 96, 117]. The highest dielectric constant was observed at around 100 °C, which might be associated with the dipolar behavior of the hydroxyl structures of the cellulose and the adsorbed/existing internal water molecules in the cellulose film [96]. The low-frequency polarization was due to the bound water, hydroxyl and the carboxyl groups [68]. Free ions or impurities will contribute to space charges in the material [123]. As the frequency increases, the space charges and permanent dipoles were relaxed. Space charges were usually the first to relax, followed by the permanent dipole groups. The presence of disordered regions gave rise to localized states associated with hydrogen bonding of cellulose chains. The release or excitation of the carriers in these states may dominate the charge transfer process. The disordered regions were mainly contributed to the dipolar orientation by stabilizing dipoles and lead to a permanent polarization which then resulted in piezoelectric behavior.

3.2 Progress in Improving the EAPap Performance

The capacity of the cellulose to be chemically modified has enabled its use as hybrid nanocomposites, such as blends or coatings, with engineered polymers, biopolymers, chitosan, carbon nanotubes and metal oxides [112, 124]. As an attempt to improve the performance of EAPap actuator, the cellulose was modified by incorporating/blending cellulose or cellulose derivatives as matrices, fillers or coatings/shells [14] with polypyrrole (PPy) or polyaniline which was used as a conductive polymer coating [124, 125], mixing carbon nanotubes with cellulose [126, 127], cellulose-chitosan blending [128, 129] and ionic liquid blending [78, 130]. The cellulose and conducting materials can be combined by various techniques such as blending, forming a co-network, or by doping [131]. Kim *et al*. [75, 124] reported that polypyrrole conducting polymer and ionic liquids could enhance the ion migration effect of cellulose, which resulted in durable bending actuation of EAPap in ambient humidity and temperature. In another work, Yun *et al*. [127, 132] mixed carbon nanotubes in the cellulose or coated the carbon nanotubes on the EAPap in an attempt to improve

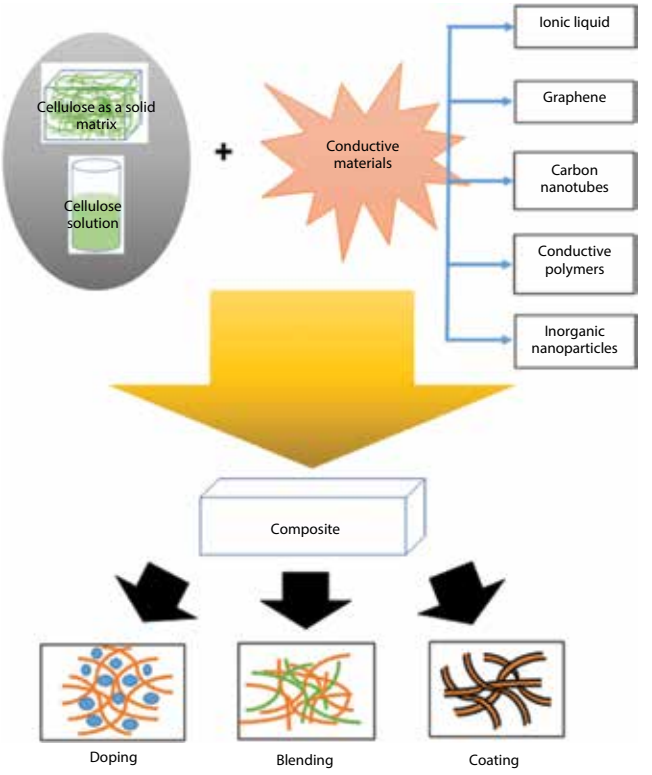

Figure 10 Schematic illustration of the generalized synthetic routes to electroconductive cellulose composites [142].

the performance of EAPap in actuation force and frequency bandwidth. Some of the synthetic routes for the hybrid EAPap are shown in Figure 10. In hybrid EAPap, the cellulose acted as a solid matrix and the electro-conductive material acted as a filler dispersed on the surface or within the matrix. Besides, cellulose was dissolved in solvents such as DMAc/LiCl, N-methylmorpholine-N-oxide (NMMO) and NaOH/urea. Alternatively, cellulose can be dissolved using ionic liquid 1-butyl-3-methylimidazolium acetate (BMIM-Ac) with conducting material to form microsphere, fibers or membranes by casting or electrospinning techniques [131].

3.2.1 Cellulose Hybrid Nanocomposites

Since the 1970s, highly conjugated polymers, such as conducting polymers with extraordinary electrical, electromechanical and optical properties, have been extensively studied [131]. The conducting polymer actuators are recognized as a material for direct drive actuators because of their large active strain and stress properties and easy manufacturing process [133]. The major advantage of using conducting polymer is the possibility to fabricate actuators in different shapes, such as films or fibers, with some desired properties [133]. In 2006, Kim *et al*. [125] reported the combination

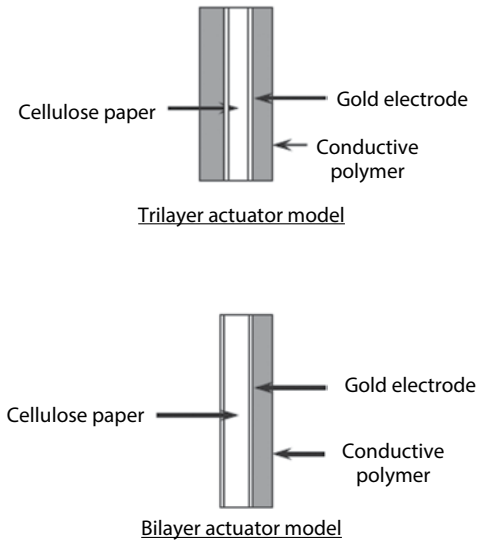

Figure 11 Bilayer and trilayer models of conductive polymer-coated EAPap [125].

of hybrid actuators with conductive polymers, such as polypyrrole and polyaniline, in cellulose. These conductive polymer-coated EAPap (CP-EAPap) actuators exhibited better performance compared to the novel EAPap. In fact, they also proved that the combination of hybrid actuators and the conductive polymer, especially polypyrrole, resulted in increased displacement due to the contraction and expansion of conductive polypyrrole layers with the presence of electric field, which enhanced the bending actuation of CP-EAPap [124]. There are two types of CP-EAPap actuators: i) CP/cellulose paper bilayers and ii) CP/cellulose trilayers [125]. The configurations of both devices are shown in Figure 11 [125]. Various reports on the studies of CP-EAPap actuators, such as polypyrrole (PPy) [125, 134] and polyaniline (PANI) [124, 135], are available. Table 3 shows the comparison of Ppy-coated EAPap and PANI-coated EAPap actuators [136]. The bending displacements of both samples were compared in the table, where the largest displacement (10.5 mm) is observed for the CP/cellulose trilayers with longer coating time. The trilayer actuators are better than the bilayer actuators due to the presence of conducting polymer on both sides. Moreover, PANI-coated actuators showed better performance than Ppy-coated actuators in bending displacement and ruggedness to humidity [124, 125]. This is simply because PANI is a better conductor than PPy and, moreover, the crystalline nature of PANI film has induced the transformation of some amorphous regions to crystalline regions in the cellulose after the actuation.

3.2.2 Cellulose-SWNT/MWNT EAPap

Carbon nanotubes (CNTs) have unique structures and exhibit excellent mechanical, thermal and electrical properties. CNTs are considered one of the most interesting nanoparticles in technology due to their many potential applications [137–139]. Due to their high conductance, high current carrying capability and small diameter in a nanoscale channel, CNTs are an ideal candidate for future nanoelectronics [127]. Shi *et al*. classified CNTs into two main categories: single-walled carbon nanotubes (SWNTs) and multiwalled carbon nanotubes (MWNTs) [131]. Single-walled carbon nanotubes consist of one single layer of graphene sheet seamlessly rolled into a cylindrical tube, while multiwalled nanotubes are made up of several concentric graphene layers [131]. Many researchers have proven that the use of SWNTs/MWNTs-cellulose hybrid actuators increase the performance of EAPap in terms of force and actuation frequency [112, 140]. Yun and Kim reported that a paper transistor made with covalently bonded multiwalled carbon nanotube and cellulose has overcome the drawbacks of low output force and low actuation frequency [139]. Studies involving CNT/cellulose composites which had excellent physical properties have been reported previously [141, 142].

In order to improve their mechanical properties, CNT was utilized in polymers [143, 144]. By introducing a small amount of CNTs into the polymer through mechanical blending or various chemical grafting methods, the CNT/polymer composites exhibited a remarkable improvement of elastic modulus and mechanical strength [136, 140]. The combinations between EAPap and multifunctionality of CNTs might improve the characteristics of the existing

Table 3 Comparison of Ppy-coated EAPap and PANI-coated EAPap actuators [79].

Conducting polymer	Configuration	dopant	Coating time (min)	Displacement (mm)
PPy coated EAPap	Bilayer	BF_{4^-}	60	5.2
	Trilayer	BF_{4^-}	90	10.5
PANI coated EAPap	Bilayer	ClO_{4^-}	45	6.7
	trilayer	BF_{4^-}	60	10.1

EAPap materials. In addition, they might also increase their application possibilities in numerous industries and in different aspects [137]. Subsequently, many researchers have focused their attention on incorporating CNTs into a polymer matrix to enhance the electrical properties of polymer from dielectric to conducting [145]. Other advantages cited in previous studies include improvement of electrochemical response in the polymer actuator [146] as well as facilitation of the dipolar alignment in piezoelectric polymer [116, 147].

The MWCNT/cellulose (M/C) composites were developed by mechanical blending and covalently grafting MWCNT with cellulose to overcome the drawbacks of EAPap [126, 127, 140]. The results showed that the reinforced mechanical property increased the resonance frequencies of EAPap to a higher band. The performance of CNTs in reinforcing the mechanical and electrical properties of cellulose has received much attention; however, other functionalities of CNTs have been neglected. For instance, homogeneous distribution of CNTs and the alignment of the CNTs covalently grafted to cellulose, which could enhance the piezoelectric property of the polymer have been neglected by researchers. MWNTs were covalently inserted into cellulose to produce M/C composites and mechanically stretched to align M/C fibers in a certain direction [115]. The stretching effect was demonstrated by observing the morphological, mechanical, electrical and piezoelectric properties of the M/C composite [115]. The MWNT is covalently grafted to the cellulose. The performance (the bending displacement) of the MWNT grafted EAPap actuator is far better than coating the MWNT onto the cellulose film alone [115]. The orientation of dipoles is established by aligning MWCNTs and cellulose chains, thus enhancing the mechanical, piezoelectric and the actuator performance of the M/C composite [115].

3.2.3 *Cellulose-Graphene Nanocomposites*

Graphene is also another impressive material due to its extraordinary high mechanical strength, high carrier mobility at room temperature, large specific area, optical transparency, and good thermal and electrical conductivity [148–150]. Graphene is a single sheet of graphite and a stable two-dimensional carbon material [131]. The mechanical properties of graphene are exceptional, i.e., the Young's modulus is 1 TPa and its ultimate strength is 130 GPa [151]. Recently, several studies on cellulose/graphene composites have been reported [152, 153]. Cellulose/graphene nanocomposite with good mechanical, dielectric and electrical properties can be produced by the synthesis of modified graphene oxide with cellulose in a well-controlled environment [153]. Feng *et al.* have highlighted the fact that graphene loading improves the electrical and mechanical properties of the composites [152]. Studies have shown that cellulose/graphene nanocomposites have many potential applications, such as in actuators, sensors, switches and artificial muscle, because of their low cost and flexibility [154–156].

Kafy *et al.* [149] synthesized cellulose/graphene nanocomposite via grafting functionalized graphene oxide onto cellulose. The nanocomposite was environmentally stable and has great potential in flexible energy storage and electronic devices [157]. Sen *et al.* also suggested that graphene nanoplatelets that were loaded into a cellulose matrix increased the mechanical, electrical and electroactive performance of cellulose/graphene nanocomposite actuators [158]. Moreover, higher concentration of graphene in polymer matrix would enhance the electrical conductivity of the cellulose film and the capability of the actuator in operating at higher excitation voltage. Thus, it produced a lower response rate of actuator [123]. Kim *et al.* prepared cellulose/graphene oxide (GO) composite films by using N-methyl-morpholine-N-oxide (NMMO) monohydrate solvents which improved the thermal, mechanical and electrical properties of the films [159]. NMMO (as solvent) can make hydrogen bonds with cellulose (matrix) and GO (filler). Thus, the three components in a solution-blend composite system have hydrogen bonding capability. A strong physical hydrogen bonding between matrix and filler is formed to a well-dispersed GO in the cellulose matrix [159]. Ozdemir *et al.* proved that the higher graphene content would escalate the value of Young's modulus of graphene loaded actuators [160]. Similarly, Zhang *et al.* showed a significant improvement in the mechanical, electrical and thermal properties of cellulose/graphene nanocomposites [161].

3.2.4 *Metal Oxide Cellulose Nanocomposites*

The introduction of metal oxides into cellulose matrix is another way of enhancing the chemical stability, conductivity and mechanical properties of cellulose [162–164]. The hybrid characteristics of the cellulose have broadened the application areas of cellulose in electronic and sensor applications. Based on the literature by Shi *et al.*, the electroplated copper hybrid cellulose-based composites displayed increased conductivity, optical, thermal and mechanical properties because of the physical or chemical interaction and synergistic effect of cellulose and copper oxide [131]. Similarly, Yadav *et al.* [165] prepared iron oxide/cellulose nanocomposite film through impregnation of iron oxide into regenerated cellulose film (see Figure 12) and the results showed that elastic modulus and tensile

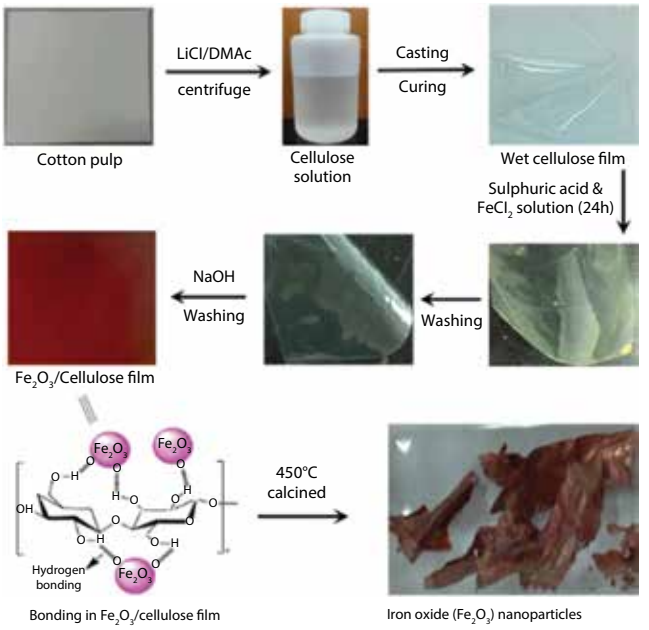

Figure 12 The procedure of preparation of Fe_2O_3/cellulose nanocomposite film [165].

strength of the cellulose film increased by 57% and 39%, respectively, compared to the regenerated cellulose.

Besides, a cellulose film coated with tin oxide (SnO_2) was developed by liquid deposition to form a flexible hybrid nanocomposite. The electrical conductivity of the nanocomposite increased with deposition time up to 4.76×10^{-3} S/cm after 24 h [166]. The SnO_2/cellulose nanocomposite has high potential for use in gas or urea sensors, lithium batteries and chemical vapor applications [166, 167]. In another study, TiO_2/cellulose nanocomposites were prepared via controlled hydrolysis of titanyl sulfate in the presence of cellulosic fibers. The nanocomposites exhibited higher opacity compared to the mechanical blending of fibers with commercial TiO_2 pigment [168]. This is because TiO_2 is highly homogeneous in its distribution and high in specific surface which is available for light scattering in the sheet containing the hybrid material [168]. Moreover, the cellulose substrates with hybrid functional metal oxides are environmentally friendly, cost-effective and have the potential to build good disposable sensor devices with better sensing performance.

Cellulose/ZnO hybrid nanocomposite exhibited superior piezoelectric property in longitudinal modes. However, it gives less efficient piezoelectric effect in bending mode [169]. The innovative research and development of the cellulose-based hybrid materials has created a great potential in the medical and bioelectronic applications because they are cheap, disposable and biocompatible with recycling facilities after disposal.

3.2.5 *Combination with Ionic Liquids*

In recent years, a group of researchers have successfully incorporated active enzymes into cellulose films using a cellulose-in-ionic-liquid dissolution and regeneration process [170]. Through this solution processing, the biomolecules were physically entrapped within the cellulose matrix and demonstrated a sustained activity [171, 172]. Several studies have proven that cellulose can be dissolved in some hydrophilic ionic liquids (ILs), such as 1-butyl-3-methylimidazolium chloride (BMIMCl) and 1-allyl-3-methylimidazolium chloride (AMIMCl) [173–175]. Dissolution of cellulose using ionic liquid has triggered high potential interest from industries and researchers due to its notable properties and abilities [176]. Properties of IL, which has low melting points, wide liquid ranges, non-volatility, high stability and polarity, high ionic conductivity, and easy recyclability, have broadened the research area in biopolymers, molecular self-assemblies and actuators [177].

The performance of EAPap was improved by using IL as a solvent for EAPap production [78, 172]. For example, the performance of bending displacement enhanced by using ionic liquid solvent 1-butyl-3-methylimidazolium hexafluorophosphate ($BMIPF_6$) showed maximum displacement output of 4 mm, which was comparatively better in the durability test for a prolonged period of time under relatively low humidity conditions [177]. A combination of conducting polymers, such as PPy and PANI with 1-butyl-3-methylimidazolium tetrafluoroborate ($BMIBF_4$) and $BMIPF_6$, improved the actuation performance of EAPap actuators [178]. The PPy and PANI operating in $BMIBF_4$ and $BMIPF_6$ exhibited larger induced strains, less polymer degradation, and less electrolyte degradation compared to the actuators operating in aqueous and organic polyelectrolytes [178]. A cellulose-PPy-IL (CPIL) nanocomposite was fabricated through the process of polymerization-induced adsorption, followed by subsequent activation in IL solutions [179]. The CPIL nanocomposites of EAPap produced a superior performance by reducing the resistance and improved the capacitance of the materials. Thus, ILs are good tools to improve the performance and durability of EAPap actuators under ambient conditions [179, 180].

4 POTENTIAL APPLICATIONS

Many unique capabilities of EAPap actuators were utilized in different applications. Some of the applications appeared to be exotic and were based on devices or systems not yet commercialized or simply not feasible using traditional actuator technologies. The low electrical power consumption of EAPap materials

is promising for accomplishing microwave-driven actuator [57]. EAPap can be utilized for sensors and actuator devices due to its excitation actuation characteristic. Cellulose-based EAPaps demonstrated high potential as biosensor due to their biocompatible and hydrophilic properties [167, 181]. The microwave-driven EAPaps can be applied in profitable innovations for remote controlled actuators, biomimetic robots, and remote detecting units [182]. In addition, EAPap indicated reasonable quality as a vibration sensor and beam vibration control [87, 90]. Acoustic characteristics of EAPap can be utilized in acoustic application [93] and EAPap is also suitable for haptic application [114].

4.1 Piezoelectric Paper Speaker

Sound is an imperative element in nature that transfers information through wave propagation of pressure created from different sources. A speaker is an electro-acoustic transducer that generates sound from an electric signal. An ordinary speaker has many different parts, i.e., voice coil with magnet, diaphragm, spiders and frame, which convert the electrical signal to sound output [183]. The interaction between magnet and voice coil will generate movement of the coil in a forward and backward manner. Volumetric space is important for different speaker designs as a component of working frequency ranges. Besides, in order to defeat the physical and structural limitations of a conventional speaker, a piezoelectric polymer such as polyvinylidene fluoride (PVDF) has been recommended to revolute the conventional speaker concept with simple structure. Cellulose as a piezoelectric paper offers promising features and characteristics for making an EAPap speaker [184]. The sound pressure level of the speaker is measured by using a microphone at the center of the speaker. The potential of piezoelectric EAPap as a thin piezoelectric speaker has been studied [116] and this has broadened the application of EAPap.

4.2 Flying Magic Paper

There are some new applications for cellulose paper for future applications like paper flying objects which can fold their wings like butterflies and pack micro-cameras with sensors for battlefield surveillance or security detection [57]. The idea came from the old-fashioned paper airplane which was played with by children in the playground and yet it can be reimagined as flying magic paper that will provide greater advantages to many industries. The discovery of cellulose as a "smart" material proved to be useful in this aspect. Development of new EAPap materials that could create large displacement has provided extraordinary value by mimicking the biological muscle that responds to an electrical stimulus which bends, flaps, and moves the material in different directions. EAPap is ultra-lightweight and consumes less energy. It has the capability of responding to electrical stimulation in a predictable way, which enables it to empower potential applications in actuators, gadgets that drive development for microscale robotic insects, tiny flying objects and wireless power supply [185].

Besides, there is no wire or battery required for sensors created from EAPap. Instead, it will be attached with extraordinary microstrip antenna called rectenna (rectifying antenna) and other lightweight electronic components. Radio waves received by the antenna will be converted into electricity which will operate the EAPap [180]. Furthermore, these actuators can be remotely driven using microwaves, e.g., microscale robotic insects, smart wallpaper, morphing wings for flying objects and microelectromechanical systems (MEMS) [57].

4.3 Biodegradable Microelectromechanical Systems (MEMS)

Generally, micromechanical system (MEMS) devices work by cooperating with at least one type of transducer, such as a sensor, generator or actuator, which operates to convert electrical energy into mechanical energy. The biggest advantage of MEMS devices is the compact and simple package with the integrated electronics and transducer of the MEMS devices. The design and performance of MEMS devices are dependent on the performance of the transducer. In this context, the new transducer advancement has a big impact on the capabilities of the existing MEMS devices. MEMS transducer is mostly electrostatic (capacitive), piezoelectric or piezoresistive when electromagnetism commands the transducers at the macroscale. Electroactive polymers are an innovative transducer which may provide numerous cutting-edge features for MEMS devices such as low cost, compatibility with different manufacturer's systems and techniques and the capability to withstand extensive environmental conditions.

With the combination of piezoelectricity and migration of ion, EAPap material will be an inexpensive and lightweight biomimetic actuator. Figure 13 illustrates the future applications of EAPap in MEM industries [183]. Nevertheless, in order to fulfill its requirements as a smart material, the characteristics and properties of cellulose needs to be explored and studied to encourage its application in numerous areas and industries. For instance, EAPap materials have been of great benefit to the entertainment industry by providing

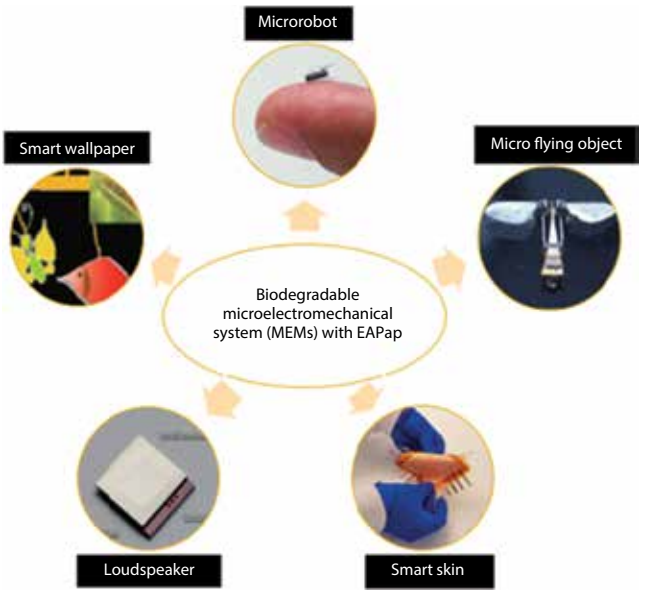

Figure 13 Applications of microwave-driven EAPap actuators [183].

attractive characteristics that produce more realistic models of living creatures at significantly lower cost [186]. The summary of the EAPap, its potential, advantages and current challenges are displayed in Table 4.

5 CONCLUSION

Lignocellulosic biomass-derived cellulose nanomaterial is a sustainable and renewable polymer with high prospects for application as a smart material in the electroactive polymer family. However, the complex structure of biomass, which is composed of cellulose, hemicellulose and lignin compounds, makes the separation process a challenging one. It involves multistep processes which include biomass pretreatment to extract cellulose fibrils from non-cellulosic compounds, followed by the preparation of cellulose in nano-dimension via different types of approaches (e.g., TEMPO oxidation or acid hydrolysis). The application of bio-based cellulose and nanocellulose

Table 4 Application of microwave-driven EAPap [109].

Application	Potential advantages of EAPap	Current EAP materials and disadvantages
Robotic or prosthetic actuators	Reconfigurable ability in novel:	– Conducting polymer wetness
	Shape: direct	
	Drive: lightweight	
	– Ability to integrate actuators and structure	
Smart skin	– Can provide new functionality in large areas area	– Shape Memory alloy film, carbon nanotubes
	– Allow large out-of-plane motions	– Microfabrication difficulty
	– Lighter and cost effective	
Loudspeaker, smart wallpaper	Flat-paper loudspeakers on walls	– Dielectric elastomers wetness
	– Active/semi-active noise suppression	– High voltage
Flapping wing	– Lightweight and low power consumption	– IPMS (Ionic Polymer-metal Composite)
	– Remote power supply	– Dielectric elastomer
	– cheap	– Wetness
		– High voltage
Entertainment industry (Portraying androids, telerobots, animatronics and animals	Offering attractive characteristics:	– Dielectric elastomer
	– provide more lifelike aesthetics, vibration and shock dampening, and more flexible actuator configurations	– High voltage
	– Realistic model of living creatures at lower cost	
MEMS (micromechanical systems)	PAPER-MEMS	None
	– Biodegradable	
	– Cheap	

in electroactive paper has been of great interest to researchers and industries in various fields. This review has summarized the principle behind the actuation of electroactive paper, the performance, material preparation and characterization, as well as the enhancement of the device performance by incorporating or modifying the material. The potential applications of electroactive paper in MEMS, sensors, actuator devices and many other applications have been thoroughly discussed in this review.

ACKNOWLEDGMENTS

The authors are grateful for the financial support from the Ministry of Science, Technology and Innovation (MOSTI) e-Science Fund (grant number SF002-2015), University of Malaya's Reseach Grant: Postgraduate Research Grant Scheme PPP (PG249-2016A), UMRG (RP026D-15AFR) and SATU Joint Research Scheme (ST015-2017). The authors would also like to thank the National Research Foundation of Korea (NRF-2015R1A3A2066301) for its support.

REFERENCES

1. J.Y. Tock, C.L. Lai, K.T. Lee, K.T. Tan, and S. Bhatia, Banana biomass as potential renewable energy resource: A Malaysian case study. *Renew. Sustainable Energy Rev.* **14**, 798–805 (2010).
2. N.L. Panwar, S.C. Kaushik, and S. Kothari, Role of renewable energy sources in environmental protection: A review. *Renew. Sustainable Energy Rev.* **15**, 1513–1524 (2011).
3. Z. Anwar, M. Gulfraz, and M. Irshad, Agro-industrial lignocellulosic biomass a key to unlock the future bio-energy: A brief review. *J. Radiat. Res. Appl. Sci.* **7**, 163–173 (2014).
4. H.C. Ong, T.M.I. Mahlia, and H.H. Masjuki, A review on energy scenario and sustainable energy in Malaysia. *Renew. Sustainable Energy Rev.* **15**, 639–647 (2011).
5. P. Gullón, E. Conde, A. Moure, H. Domínguez, and J.C. Parajó, Selected process alternatives for biomass refining: A review. *Open Agr. J.* **4**, 135–144 (2010).
6. T. Shahzadi, S. Mehmood, M. Irshad, Z. Anwar, A. Afroz, N. Zeeshan, and K. Sughra, Advances in lignocellulosic biotechnology: A brief review on lignocellulosic biomass and cellulases. *Adv. Biosci. Biotechnol.* **5**, 246–251 (2014).
7. H. Lee, S. Hamid, and S. Zain, Conversion of lignocellulosic biomass to nanocellulose: Structure and chemical process. *Scientific World J.* **2014**, 631013 (2014).
8. F. Cherubini, The biorefinery concept: Using biomass instead of oil for producing energy and chemicals. *Energ. Convers. Manage.* **51**, 1412–1421 (2010).
9. H. Chen, Chemical composition and structure of natural lignocellulose, in *Biotechnology of Lignocellulose: Theory and Practice*, H.Z. Chen (Ed.), pp. 25–71, Springer, Netherlands, Dordrecht (2014).
10. C.J. Chirayil, L. Mathew, and S. Thomas, Review of recent research in nano cellulose preparation from different lignocellulosic fibres. *Rev. Adv. Mater. Sci.* **37**, 20–28 (2014).
11. V. Balan, Current challenges in commercially producing biofuels from lignocellulosic biomass. *Int. Sch. Res. Notices* **2014**, 463074 (2014).
12. D. Watkins, M. Nuruddin, M. Hosur, A. Tcherbi-Narteh, and S. Jeelani, Extraction and characterization of lignins from different biomass resources. *J. Mater. Res. Technol.* **4**, 26–32 (2015).
13. E.E. Tănase, M. Râpă, and O. Popa, Biopolymers based on renewable resources—A review. *Scientific Bulletin. Series F. Biotechnologies* **XVIII**, 188–195 (2014).
14. X. Qiu and S. Hu, "Smart" materials based on cellulose: A review of the preparations, properties, and applications. *Materials* **6**, 738–781 (2013).
15. H.P.S. Abdul Khalil, A.H. Bhat, and A.F. Ireana Yusra, Green composites from sustainable cellulose nanofibrils: A review. *Carbohydr. Polym.* **87**, 963–979 (2012).
16. T. Huber, J. Müssig, O. Curnow, S. Pang, S. Bickerton, and M. P. Staiger, A critical review of all-cellulose composites. *Adv. Mater. Res.* **47**, 1171–1186 (2011).
17. S. Kalia, A. Dufresne, B.M. Cherian, B. Kaith, L. Avérous, J. Njuguna, and E. Nassiopoulos, Cellulose-based bio-and nanocomposites: A review. *Int. J. Polym. Sci.* **2011**, 837875 (2011).
18. H.A. Khalil, Y. Davoudpour, M.N. Islam, A. Mustapha, K. Sudesh, R. Dungani, and M. Jawaid, Production and modification of nanofibrillated cellulose using various mechanical processes: A review. *Carbohydr. Polym.* **99**, 649–665 (2014).
19. M. Börjesson and G. Westman, Crystalline nanocellulose — Preparation, modification, and properties, in *Cellulose: Fundamental Aspects and Current Trends*, M. Poletto and H.L. Ornaghi Jr. (Ed.), pp. 159–191, INTECH Open Access Publisher, London (2015).
20. M. Henriksson, L.A. Berglund, P. Isaksson, T. Lindström, and T. Nishino, Cellulose nanopaper structures of high toughness. *Biomacromolecules* **9**, 1579–1585 (2008).
21. O. Nechyporchuk, M.N. Belgacem, and J. Bras, Production of cellulose nanofibrils: A review of recent advances. *Ind. Crops. Prod.* **93**, 2–25 (2016).
22. F. Li, E. Mascheroni and L. Piergiovanni, The potential of nanocellulose in the packaging field: A review. *Packag. Technol. Sci.* **28**, 475–508 (2015).
23. F. Jiang and Y.-L. Hsieh, Chemically and mechanically isolated nanocellulose and their self-assembled structures. *Carbohydr. Polym.* **95**, 32–40 (2013).
24. N. Lin and A. Dufresne, Nanocellulose in biomedicine: Current status and future prospect. *Eur. Polym. J.* **59**, 302–325 (2014).
25. A. García, A. Gandini, J. Labidi, N. Belgacem, and J. Bras, Industrial and crop wastes: A new source for nanocellulose biorefinery. *Ind. Crops. Prod.* **93**, 26–38 (2016).

26. E. Abraham, B. Deepa, L. Pothan, M. Jacob, S. Thomas, U. Cvelbar, and R. Anandjiwala, Extraction of nanocellulose fibrils from lignocellulosic fibres: A novel approach. *Carbohydr. Polym.* **86**, 1468–1475 (2011).
27. P. Harmsen, W. Huijgen, L. Bermudez, and R. Bakker, *Literature Review of Physical and Chemical Pretreatment Processes for Lignocellulosic: Biomass*, pp. 1–49, Energy Research Center of the Netherlands, North Holland (2010).
28. N. Mosier, C. Wyman, B. Dale, R. Elander, Y. Lee, M. Holtzapple, and M. Ladisch, Features of promising technologies for pretreatment of lignocellulosic biomass. *Bioresour. Technol.* **96**, 673–686 (2005).
29. I.-K. Yang and C.-H. Wu, Real-time SAXS measurements and rheological behavior of poly(lactic acid) crystallization under continuous shear flow. *J. Polym. Res.* **21**, 609–623 (2014).
30. H. Lu, Y. Gui, L. Zheng, and X. Liu, Morphological, crystalline, thermal and physicochemical properties of cellulose nanocrystals obtained from sweet potato residue. *Food Res. Int.* **50**, 121–128 (2013).
31. F.H. Isikgor and C.R. Becer, Lignocellulosic biomass: A sustainable platform for the production of bio-based chemicals and polymers. *Polym. Chem.* **6**, 4497–4559 (2015).
32. S. Naseeruddin, S. Desai, and L. Venkateswar Rao, Selection of suitable mineral acid and its concentration for biphasic dilute acid hydrolysis of the sodium dithionite delignified *Prosopis juliflora* to hydrolyze maximum holocellulose. *Bioresour. Technol.* **202**, 231–237 (2016).
33. D. Humbird, R. Davis, L. Tao, C. Kinchin, D. Hsu, A. Aden, P. Schoen, J. Lukas, B. Olthof, M. Worley, D. Sexton, and D. Dudgeon, *Process Design and Economics for Biochemical Conversion of Lignocellulosic Biomass to Ethanol: Dilute-Acid Pretreatment and Enzymatic Hydrolysis of Corn Stover*, Medium: ED Size, pp. 147, National Renewable Energy Laboratory, Golden, CO (2011).
34. Y.-L. Loow, T. Y. Wu, J. Md Jahim, and A. Mohammad, Using dilute acid hydrolysis pre-treatment in transforming lignocellulosic biomass into reducing sugars: A review, in *Asia Pacific Confederation of Chemical Engineering Congress 2015: APCChE 2015*, incorporating CHEMECA 2015, 1428, Melbourne, Engineers Australia (2015).
35. P. Lenihan, A. Orozco, E. O'Neill, M. Ahmad, D. Rooney, and G. Walker, Dilute acid hydrolysis of lignocellulosic biomass. *Chem. Eng. J.* **156**, 395–403 (2010).
36. S. Satimanont, A. Luengnaruemitchai, and S. Wongkasemjit, Effect of temperature and time on dilute acid pretreatment of corn cobs. *Int. J. Chem. Biol. Eng.* **6(4)**, 316–320 (2012).
37. K. Uetani and H. Yano, Nanofibrillation of wood pulp using a high-speed blender. *Biomacromolecules* **12**, 348–353 (2011).
38. B.-W. Koo, B.-C. Min, K.-S. Gwak, S.-M. Lee, J.-W. Choi, H. Yeo, and I.-G. Choi, Structural changes in lignins during organosolv pretreatment of *Liriodendron tulipifera* and the effect on enzymatic hydrolysis. *Biomass Bioenerg.* **42**, 24–32 (2012).
39. S.-K. Jang, H.-Y. Kim, H.-S. Jeong, J.-Y. Kim, H. Yeo, and I.-G. Choi, Effect of ethanol organosolv pretreatment factors on enzymatic digestibility and ethanol organosolv lignins structure from *Liriodendron tulipifera* in specific combined severity factors. *Renew. Energy* **87**, 599–606 (2016).
40. A. Isogai, T. Saito, and H. Fukuzumi, TEMPO-oxidized cellulose nanofibers. *Nanoscale* **3**, 71–85 (2011).
41. H. Fukuzumi, T. Saito, and A. Isogai, Influence of TEMPO-oxidized cellulose nanofibril length on film properties. *Carbohydr. Polym.* **93**, 172–177 (2013).
42. S. Fujisawa, Y. Okita, H. Fukuzumi, T. Saito, and A. Isogai, Preparation and characterization of TEMPO-oxidized cellulose nanofibril films with free carboxyl groups. *Carbohydr. Polym.* **84**, 579–583 (2011).
43. B. Deepa, E. Abraham, N. Cordeiro, M. Mozetic, A.P. Mathew, K. Oksman, M. Faria, S. Thomas, and L.A. Pothan, Utilization of various lignocellulosic biomass for the production of nanocellulose: A comparative study. *Cellulose* **22**, 1075–1090 (2015).
44. T. Saito, M. Hirota, N. Tamura, S. Kimura, H. Fukuzumi, L. Heux, and A. Isogai, Individualization of nano-sized plant cellulose fibrils by direct surface carboxylation using TEMPO catalyst under neutral conditions. *Biomacromolecules* **10**, 1992–1996 (2009).
45. J. Huang, P.R. Chang, N. Lin, and A. Dufresne, *Polysaccharide-Based Nanocrystals: Chemistry and Applications*, John Wiley & Sons, New Jersey (2014).
46. Y. Okita, T. Saito, and A. Isogai, Entire surface oxidation of various cellulose microfibrils by TEMPO-mediated oxidation. *Biomacromolecules* **11**, 1696–1700 (2010).
47. R. Tanaka, T. Saito, and A. Isogai, Cellulose nanofibrils prepared from softwood cellulose by TEMPO/NaClO/NaClO2 systems in water at pH 4.8 or 6.8. *Int. J. Biol. Macromol.* **51**, 228–234 (2012).
48. H. Fukuzumi, Studies on structures and properties of TEMPO-oxidized cellulose nanofibril films. pp. 1–88, Thesis (2012).
49. R. Shinoda, T. Saito, Y. Okita, and A. Isogai, Relationship between length and degree of polymerization of TEMPO-oxidized cellulose nanofibrils. *Biomacromolecules* **13**, 842–849 (2012).
50. F. Jiang, S. Han, and Y.-L. Hsieh, Controlled defibrillation of rice straw cellulose and self-assembly of cellulose nanofibrils into highly crystalline fibrous materials. *RSC Adv.* **3**, 12366–12375 (2013).
51. L. Dai, Z. Long, Y. Lv, and Q. Feng, The role of formic acid pretreatment in improving the carboxyl content of TEMPO-oxidized cellulose. *Cellulose Chem. Technol.* **5**, 469–475 (2014).
52. F. Bettaieb, O. Nechyporchuk, R. Khiari, M.F. Mhenni, A. Dufresne, and M.N. Belgacem, Effect of the oxidation treatment on the production of cellulose nanofiber suspensions from *Posidonia oceanica*: The rheological aspect. *Carbohydr. Polym.* **134**, 664–672 (2015).
53. A.A. Oun and J.-W. Rhim, Characterization of nanocelluloses isolated from Ushar (*Calotropis procera*) seed

fiber: Effect of isolation method. *Mater. Lett.* **168**, 146–150 (2016).
54. X. Miao, J. Lin, F. Tian, X. Li, F. Bian, and J. Wang, Cellulose nanofibrils extracted from the byproduct of cotton plant. *Carbohydr. Polym.* **136**, 841–850 (2016).
55. Q. Meng, S. Fu, and L.A. Lucia, The role of heteropolysaccharides in developing oxidized cellulose nanofibrils. *Carbohydr. Polym.* **144**, 187–195 (2016).
56. I. Siró and D. Plackett, Microfibrillated cellulose and new nanocomposite materials: A review. *Cellulose* **17**, 459–494 (2010).
57. T. Saito, S. Kimura, Y. Nishiyama, and A. Isogai, Cellulose nanofibers prepared by TEMPO-mediated oxidation of native cellulose. *Biomacromolecules* **8**, 2485–2491 (2007).
58. M. Nogi, S. Iwamoto, A.N. Nakagaito, and H. Yano, Optically transparent nanofiber paper. *Adv. Mater.* **21**, 1595–1598 (2009).
59. K. Nagashima, H. Koga, U. Celano, F. Zhuge, M. Kanai, S. Rahong, G. Meng, Y. He, J.D. Boeck, M. Jurczak, W. Vandervorst, T. Kitaoka, M. Nogi, and T. Yanagida, Cellulose nanofiber paper as an ultra flexible nonvolatile memory. *Sci. Rep.* **4**, 5532 (2014.).
60. M. Nogi and H. Yano, Transparent nanocomposites based on cellulose produced by bacteria offer potential innovation in the electronics device industry. *Adv. Mater.* **20**, 1849–1852 (2008).
61. J. Shah and R.M. Brown Jr., Towards electronic paper displays made from microbial cellulose. *Appl. Microbiol. Biotechnol.* **66**, 352–355 (2005).
62. M. Stigter, J. Bezemer, K. De Groot, and P. Layrolle, Incorporation of different antibiotics into carbonated hydroxyapatite coatings on titanium implants, release and antibiotic efficacy. *J. Control. Release* **99**, 127–137 (2004).
63. F.A. Müller, L. Müller, I. Hofmann, P. Greil, M.M. Wenzel, and R. Staudenmaier, Cellulose-based scaffold materials for cartilage tissue engineering. *Biomaterials* **27**, 3955–3963 (2006).
64. J. Li, Y. Wan, L. Li, H. Liang, and J. Wang, Preparation and characterization of 2,3-dialdehyde bacterial cellulose for potential biodegradable tissue engineering scaffolds. *Mater. Sci. Eng. C* **29**, 1635–1642 (2009).
65. J. Giri and R. Adhikari, A brief review on extraction of nanocellulose and its application. *Bibechana* **9**, 81–87 (2012).
66. M. Jorfi and E.J. Foster, Recent advances in nanocellulose for biomedical applications. *J. Appl. Polym. Sci.* **132**, 41719 (2015).
67. S. Yun, S. Jang, G.-Y. Yun, and J. Kim, Electrically aligned cellulose film for electro-active paper and its piezoelectricity. *Smart Mater. Struct.* **18**, 117001 (2009).
68. J. Kim, S. Yun, and Z. Ounaies, Discovery of cellulose as a smart material. *Macromolecules* **39**, 4202–4206 (2006).
69. M. Mohiuddin, A. Akther, E.B. Jo, H.C. Kim, and J. Kim, Fabrication and finite element analysis of vibrating parallel film actuator made with cellulose acetate for potential haptic application. *Proc. Inst. Mech. Eng. C: J. Mech. Eng. Sci.* **230**, 2720–2727 (2015).
70. J. Kim, C.-S. Song, and S.-R. Yun, Cellulose based electro-active papers: Performance and environmental effects. *Smart Mater. Struct.* **15**, 719–723 (2006).
71. J. Kim and Y.B. Seo, Electro-active paper actuators. *Smart Mater. Struct.* **11**, 355–360 (2002).
72. G. Zheng, Y. Cui, E. Karabulut, L. Wågberg, H. Zhu, and L. Hu, Nanostructured paper for flexible energy and electronic devices. *MRS Bull.* **38**, 320–325 (2013).
73. J. Kim, W. Jung, and H.S. Kim, In-plane strain of electro-active paper under electric fields. *Sens. Actuators A Phys.* **140**, 225–231 (2007).
74. J.H. Kim, Y.K. Kang, and S.R. Yun, Characterization of electro-active paper composite. *Key Eng. Mater.* **297–300**, 671–675 (2005).
75. J.H. Kim, S.R. Yun, S.K. Mahadeva, K. Yun, S.Y. Yang, and M. Maniruzzaman, Paper actuators made with cellulose and hybrid materials. *Sensors* **10**, 14731485 (2010).
76. J.-H. Kim, S.-W. Lee, G.-Y. Yun, C. Yang, H.S. Kim, and J. Kim, Observation of creep behavior of cellulose electro-active paper (EAPap) actuator, in *SPIE Smart Structures and Materials + Nondestructive Evaluation and Health Monitoring*, vol. 7289, pp. 1–7, Society of Photographic Instrumentation Engineers, Bellingham (2009).
77. J. Kim, Y. Kang, and S. Yun, Blocked force measurement of electro-active paper actuator by micro-balance. *Sens. Actuators A Phys.* **133**, 401–406 (2007).
78. S.K. Mahadeva, C. Yi, and J. Kim, Effect of room temperature ionic liquids adsorption on electromechanical behavior of cellulose electro-active paper. *Macromol. Res.* **17**, 116–120 (2009).
79. H.S. Kim, J. Kim, W. Jung, J. Ampofo, W. Craft, and J. Sankar, Mechanical properties of cellulose electro-active paper under different environmental conditions. *Smart Mater. Struct.* **17**, 015029 (2008).
80. J. Kim, S. Yun, and S.-K. Lee, Cellulose smart material: Possibility and challenges. *J. Intell. Mater. Syst. Struct.* **19**, 417–422 (2008).
81. R.J. Moon, A. Martini, J. Nairn, J. Simonsen, and J. Youngblood, Cellulose nanomaterials review: Structure, properties and nanocomposites. *Chem. Soc. Rev.* **40**, 3941–3994 (2011).
82. R. Parthasarathi, K. Balamurugan, J. Shi, V. Subramanian, B.A. Simmons, and S. Singh, Theoretical insights into the role of water in the dissolution of cellulose using IL/water mixed solvent systems. *J. Phys. Chem. B* **119**, 14339–14349 (2015).
83. M. Shahinpoor, Ionic polymer metal composites as dexterous manipulators and haptic feedback/tactile sensors for minimally invasive robotic surgery, in *Ionic Polymer Metal Composites (IPMCs): Smart Multi-Functional Materials and Artificial Muscles*, M. Shahinpoor (Ed.), vol. 2, pp. 311–340, Royal Society of Chemistry, London (2015).
84. J. Kim, M. Maniruzaman, S.R. Yun, and S.Y. Yang, Cellulose smart material: Its principle and applications. DTIC Document (2010).
85. J.-H. Kim, K.-J. Yun, J.-H. Kim, and J. Kim, Mechanical stretching effect on the actuator performance of

cellulose electroactive paper. *Smart Mater. Struct.* **18**, 055005 (2009).
86. S. Yun, J. Kim, and K.-S. Lee, Evaluation of cellulose electro-active paper made by tape casting and zone stretching methods. *Int. J. Precis. Eng. Man.* **11**, 987–990 (2010).
87. S.-W. Lee, J.-H. Kim, J. Kim, and H.S. Kim, Characterization and sensor application of cellulose electro-active paper (EAPap). *Chin. Sci. Bull.* **54**, 2703–2707 (2009).
88. D. Klemm, B. Heublein, H.-P. Fink, and A. Bohn, Cellulose: Fascinating biopolymer and sustainable raw material. *Angew. Chem. Int. Ed. Engl.* **44**, 3358–3393 (2005).
89. C. Yang, J.-H. Kim, J. Kim, and H.S. Kim, Piezoelectricity of wet drawn cellulose electro-active paper. *Sens. Actuators A Phys.* **154**, 117–122 (2009).
90. J. Kim, H. Lee, and H.S. Kim, Beam vibration control using cellulose-based electro-active paper sensor. *Int. J. Precis. Eng. Man.* **11**, 823–827 (2010).
91. L. Zhai, B.W. Kang, J.H. Kim, J. Kim, Z. Abas, and H.S. Kim, Electrode effect on the cellulose piezo-paper energy harvester, in *SPIE Smart Structures and Materials + Nondestructive Evaluation and Health Monitoring*, vol. 8687, pp. 1–4, Society of Photographic Instrumentation Engineers, Bellingham (2013).
92. L. Zhai, B.-W. Kang, J.-H. Kim, J. Kim, Z. Abas, and H.S. Kim, Cellulose electro-active paper fabricated by facile solvent exchange pretreatment and its physical and electromechanical properties. *Cellulose* **22**, 927–933 (2015).
93. J. Kim, G.Y. Yun, J.H. Kim, J. Lee, and J. Kim, Piezoelectric electro-active paper (EAPap) speaker. *J. Mech. Sci. Technol.* **25**, 2763–2768 (2011).
94. Z. Abas, H.S. Kim, L. Zhai, J. Kim, and J.H. Kim, Electrode effects of a cellulose-based electro-active paper energy harvester. *Smart Mater. Struct.* **23**, 074003 (2014).
95. J.-H. Kim, K. Kang, S. Yun, S. Yang, M.-H. Lee, J.-H. Kim, and J. Kim, Cellulose electroactive paper (EAPap): The potential for a novel electronic material, in *MRS Proceedings*, vol. 1129, pp. 1129–V05, Cambridge University Press, Cambridge (2008).
96. G.-Y. Yun, J.-H. Kim, and J. Kim, Dielectric and polarization behaviour of cellulose electro-active paper (EAPap). *J. Phys. D: Appl. Phys.* **42**, 082003 (2009).
97. Y. Gyu-young, K. Heung Soo, and K. Jaehwan, Blocked force measurement of an electro-active paper actuator using a cantilevered force transducer. *Smart Mater. Struct.* **17**, 025021 (2008).
98. H.S. Kim, Y. Li, and J. Kim, Electro-mechanical behavior and direct piezoelectricity of cellulose electro-active paper. *Sens. Actuators A Phys. Sensors.* **147**, 304–309 (2008).
99. J. Kim, J. Ampofo, W. Craft, and Soo Kim, Modeling elastic, viscous and creep characteristics of cellulose electro-active paper. *Mech. Mater.* **40**, 1001–1011 (2008).
100. M. Ishihara, Y. Ootao, and Y. Kameo, A general solution technique for electroelastic fields in piezoelectric bodies with D ∞ symmetry in cylindrical coordinates. *J. Wood Sci.* **62**, 29–41 (2016).
101. E. Fukada, History and recent progress in piezoelectric polymers. *IEEE Trans. Ultrason. Ferroelectr. Freq. Control* **47**, 1277–1290 (2000).
102. J. Kim, Improvement of piezoelectricity in piezoelectric paper made with cellulose. DTIC Document (2009).
103. L. Csoka, I.C. Hoeger, O.J. Rojas, I. Peszlen, J.J. Pawlak, and P.N. Peralta, Piezoelectric effect of cellulose nanocrystals thin films. *ACS Macro Lett.* **1**, 867–870 (2012).
104. J.-H. Kim, S. Yun, and J. Kim, Fabrication of piezoelectric cellulose paper and audio application. *J. Bionic Eng.* **6**, 18–21 (2009).
105. Z. Abas, H.S. Kim, J. Kim, and J.-H. Kim, Cellulose electro-active paper: From discovery to technology applications. *Frontiers in Materials* **1**, 1–4 (2014).
106. L.J. Zhao and Q. Fu. Parametric study of EAPap material properties, in *Frontiers of Advanced Materials and Engineering Technology*, R. Chen, D.G. Sun, and W.P. Sung (Eds.), pp. 242–246, Trans Tech Publications, Switzerland (2012).
107. S.K. Mahadeva, S.-W. Lee, and J. Kim, Effect of heat treatment on the structure, piezoelectricity and actuation behavior of a cellulose electroactive-paper actuator. *Acta Mater.* **56**, 1868–1875 (2008).
108. S.K. Mahadeva, K. Walus, and B. Stoeber, Paper as a platform for sensing applications and other devices: A review. *ACS Appl. Mater. Interfaces* **7**, 8345–8362 (2015).
109. W. Czaja, A. Krystynowicz, M. Kawecki, K. Wysota, S. Sakiel, P. Wróblewski, J. Glik, M. Nowak, and S. Bielecki, Biomedical applications of microbial cellulose in burn wound recovery, in *Cellulose: Molecular and Structural Biology*, R.M. Brown Jr. and I.M. Saxena (Eds.), pp. 307–321, Springer, New York (2007).
110. S. Lee, J.H. Kim, K. Kang, J. Kim, H.S. Kim, and C. Yang, Characterization of micro-scale creep deformation of an electro-active paper actuator. *Smart Mater. Struct.* **18**, 095008 (2009).
111. H.S. Kim, J. Kim, W. Jung, J. Ampofo, W. Craft, and J. Sankar, Mechanical properties of cellulose-based electro-active paper. *Proc. Inst. Mech. Eng. C J. Mech. Eng. Sci.* **222**, 577–583 (2008).
112. A. Khan, Z. Abas, H. Kim, and J. Kim, Recent progress on cellulose-based electro-active paper, its hybrid nanocomposites and applications. *Sensors* **16**, 1172 (2016).
113. S.R. Yun, G.Y. Yun, J.H. Kim, Y. Chen, and J. Kim, Electro-active paper for a durable biomimetic actuator. *Smart Mater. Struct.* **18**, 024001 (2009).
114. G.-Y. Yun, J. Kim, J.-H. Kim, and S.-Y Kim, Fabrication and testing of cellulose EAPap actuators for haptic application. *Sens. Actuators A Phys.* **164**, 68–73 (2010).
115. S.-Y. Yang, J.-H. Kim, and K.-D. Song, Flexible patch rectennas for wireless actuation of cellulose electro-active paper actuator. *J. Electr. Eng. Technol.* **7**, 954–958 (2012).
116. S. Yun and J. Kim, Mechanical, electrical, piezoelectric and electro-active behavior of aligned multi-walled

carbon nanotube/cellulose composites. *Carbon* **49**, 518–527 (2011).
117. G.Y. Yun, H.S. Kim, J.H. Kim, K. Kim, and C. Yang, Effect of aligned cellulose film to the performance of electro-active paper actuator. *Sens. Actuators A Phys.* **141**(2), 530–535 (2008)..
118. S.R. Yun, Y. Chen, J.N. Nayak, and J.H. Kim, Effect of solvent mixture on properties and performance of electro-active paper made with regenerated cellulose. *Sens. Actuators B Chem.* **129**, 652–658 (2008).
119. H.S. Kim, S.R. Yun, J.H. Kim, G.Y. Yun, and J. Kim, Fabrication and characterization of piezo-paper made with cellulose. The 15th International Symposium on Smart Structures and Materials & Nondestructive Evaluation and Health Monitoring. *International Society for Optics and Photonics*, **6929**, 69290O-1-7(2008).
120. J. Kim, Cellulose as a smart material, in *Cellulose: Molecular and Structural Biology*, R.M. Brown, Jr. and I.M. Saxena (Eds.), pp. 323–343, Springer, Netherlands (2007).
121. N.-G. Wang, J. Kim, Y. Chen, S.-R. Yun, and S.-K. Lee, Electro-active-paper actuator made with LiCl/cellulose films: Effect of LiCl content. *Macromol. Res.* **14**, 624–629 (2006).
122. B. Akle and D.J. Leo, Electromechanical transduction in multilayer ionic transducers. *Smart Mater. Struct.* **13**, 1081–1089 (2004).
123. J. Kim, S. Mun, H.-U. Ko, L. Zhai, S.-K. Min, and H.C. Kim, A comprehensive review of electroactive paper actuators, in *Ionic Polymer Metal Composites (IMPCs): Smart Multi-Functional Materials and Artificial Muscles*, M. Shahinpoor (Ed.), vol. 2, pp. 386–398, Royal Society of Chemistry, Cambridge (2015).
124. J. Kim, S.R. Yun, and S.D. Deshpande, Synthesis, characterization and actuation behavior of polyaniline-coated electroactive paper actuators. *Polym. Int.* **56**, 1530–1536 (2007).
125. J. Kim, S. Deshpande, S. Yun, and Q. Li, A comparative study of conductive polypyrrole and polyaniline coatings on electro-active papers. *Polym. J.* **38**, 659–668 (2006).
126. S. Yun and J. Kim, Characteristics and performance of functionalized MWNT blended cellulose electro-active paper actuator. *Synth. Met.* **158**, 521–526 (2008).
127. S. Yun and J. Kim, A bending electro-active paper actuator made by mixing multi-walled carbon nanotubes and cellulose. *Smart Mater. Struct.* **16**, 1471–1476 (2007).
128. Z. Cai and J. Kim, Characterization and electromechanical performance of cellulose–chitosan blend electroactive paper. *Smart Mater. Struct.* **17**, 035028 (2008).
129. N. Wang, Y. Chen, and J. Kim, Electroactive paper actuator made with chitosan-cellulose films: Effect of acetic acid. *Macromol. Mater. Eng.* **292**, 748–753 (2007).
130. S.K. Mahadeva and J. Kim, Electromechanical behavior of room temperature ionic liquid dispersed cellulose. *J. Phys. Chem.* **113**, 12523–12529 (2009).
131. Z. Shi, G.O. Phillips, and G. Yang, Nanocellulose electroconductive composites. *Nanoscale* **5**, 3194–3201 (2013).
132. S. Yun, J. Kim, and Z. Ounaies, Single-walled carbon nanotube/polyaniline coated cellulose based electroactive paper (EAPap) as hybrid actuator. *Smart Mater. Struct.* **15**, N61–N65 (2006).
133. S.D. Deshpande, J. Kim, and S.R. Yun, Studies on conducting polymer electroactive paper actuators: Effect of humidity and electrode thickness. *Smart Mater. Struct.* **14**, 876–880 (2005).
134. S.Y. Yang, S.K. Mahadeva, and J. Kim, Wirelessly driven electro-active paper actuator made with cellulose–polypyrrole–ionic liquid and dipole rectenna. *Smart Mater. Struct.* **19**, 105026 (2010).
135. H.-U. Ko, S.C. Mun, L. Zhai, K.-B. Kim, and J. Kim, Performance characterization of polyaniline coated electro-active paper actuator. *J. Korean Soc. Precis. Eng.* **30**, 658–664 (2013).
136. H. Qi, J. Liu, and E. Mäder, Smart cellulose fibers coated with carbon nanotube networks. *Fibers* **2**, 295–307 (2014).
137. E.T. Thostenson and T.W. Chou, Carbon nanotube networks: Sensing of distributed strain and damage for life prediction and self healing. *Adv. Mater.* **18**, 2837–2841 (2006).
138. D. Ferrer, T. Tanii, I. Matsuya, G. Zhong, S. Okamoto, H. Kawarada, T. Shinada, and I. Ohdomari, Enhancement of field emission characteristics of tungsten emitters by single-walled carbon nanotube modification. *Appl. Phys. Lett.* **88**, 033116 (2006).
139. S. Yun and J. Kim, Covalently bonded multi-walled carbon nanotubes-cellulose electro-active paper actuator. *Sens. Actuators A Phys.* **154**, 73–78 (2009).
140. S. Yun, S.-D. Jang, G.-Y. Yun, J.-H. Kim, and J. Kim, Paper transistor made with covalently bonded multi-walled carbon nanotube and cellulose. *Appl. Phys. Lett.* **95**, 104102 (2009).
141. R.E. Anderson, J. Guan, M. Ricard, G. Dubey, J. Su, G. Lopinski, G. Dorris, O. Bourne, and B. Simard, Multifunctional single-walled carbon nanotube–cellulose composite paper. *J. Mater. Chem.* **20**, 2400–2407 (2010).
142. M.S. Dresselhaus and M. Endo, Relation of carbon nanotubes to other carbon materials, in *Carbon Nanotubes*, M.S. Dresselhaus, G. Dresselhaus, and P. Avouris (Eds.), pp. 11–28, Springer, Berlin (2001).
143. Y. Sabba and E. Thomas, High-concentration dispersion of single-wall carbon nanotubes. *Macromolecules* **37**, 4815–4820 (2004).
144. S. Ruan, P. Gao, X.G. Yang, and T. Yu, Toughening high performance ultrahigh molecular weight polyethylene using multiwalled carbon nanotubes. *Polymer* **44**, 5643–5654 (2003).
145. C. Ma, W. Zhang, Y. Zhu, L. Ji, R. Zhang, N. Koratkar and J. Liang, Alignment and dispersion of functionalized carbon nanotubes in polymer composites induced by an electric field. *Carbon* **46**, 706–720 (2008).
146. Y.-H. Yun, V. Shanov, M.J. Schulz, S. Narasimhadevara, S. Subramaniam, D. Hurd, and F.J. Boerio, Development of novel single-wall carbon nanotube–epoxy composite ply actuators. *Smart Mater. Struct.* **14**, 1526–1532 (2005).

147. Z. Ounaies, C. Park, J. Harrison, and P. Lillehei, Evidence of piezoelectricity in SWNT-polyimide and SWNT-PZT-polyimide composites. *J. Thermoplast. Compos. Mater.* **21**, 393–409 (2008).
148. A.A. Balandin, S. Ghosh, W. Bao, I. Calizo, D. Teweldebrhan, F. Miao, and C.N. Lau, Superior thermal conductivity of single-layer graphene. *Nano Lett.* **8**, 902–907 (2008).
149. A. Kafy, K.K. Sadasivuni, A. Akther, S.-K. Min, and J. Kim, Cellulose/graphene nanocomposite as multifunctional electronic and solvent sensor material. *Mater. Lett.* **159**, 20–23 (2015).
150. V. Singh, D. Joung, L. Zhai, S. Das, S.I. Khondaker, and S. Seal, Graphene based materials: Past, present and future. *Prog. Mater. Sci.* **56**, 1178–1271 (2011).
151. C. Lee, X. Wei, J.W. Kysar, and J.T. Hone, Measurement of the elastic properties and intrinsic strength of monolayer graphene. *Science* **321**, 385–388 (2008).
152. Y. Feng, X. Zhang, Y. Shen, K. Yoshino, and W. Feng, A mechanically strong, flexible and conductive film based on bacterial cellulose/graphene nanocomposite. *Carbohydr. Polym.* **87**, 644–649 (2012).
153. H.C. Kim, S.C. Mun, H.U. Ko, L. Zhai, A. Kafy, and J. Kim, Renewable smart materials. *Smart Mater. Struct.* **25**, 073001 (2016).
154. Y. Zhao, L. Song, Z. Zhang, and L. Qu, Stimulus-responsive graphene systems towards actuator applications. *Energy Environ. Sci.* **6**, 3520–3536 (2013).
155. D. Ponnamma, Q. Guo, I. Krupa, M.A.S. Al-Maadeed, K. Varughese, S. Thomas, and K.K. Sadasivuni, Graphene and graphitic derivative filled polymer composites as potential sensors. *Phys. Chem. Chem. Phys.* **17**, 3954–3981 (2015).
156. D. Ponnamma, K.K. Sadasivuni, M. Strankowski, Q. Guo, and S. Thomas, Synergistic effect of multi walled carbon nanotubes and reduced graphene oxides in natural rubber for sensing application. *Soft Matter* **9**, 10343–10353 (2013).
157. A. Kafy, K.K. Sadasivuni, H.-C. Kim, A. Akther, and J. Kim, Designing flexible energy and memory storage materials using cellulose modified graphene oxide nanocomposites. *Phys. Chem. Chem. Phys.* 17, 5923–5931 (2015).
158. I. Sen, Y. Seki, M. Sarikanat, L. Cetin, B.O. Gurses, O. Ozdemir, O.C. Yilmaz, K. Sever, E. Akar, and O. Mermer, Electroactive behavior of graphene nanoplatelets loaded cellulose composite actuators. *Compos. Part B Eng.* **69**, 369–377 (2015).
159. C.-J. Kim, W. Khan, D.-H. Kim, K.-S. Cho, and S.-Y. Park, Graphene oxide/cellulose composite using NMMO monohydrate. *Carbohydr. Polym.* **86**, 903–909 (2011).
160. O. Ozdemir, R. Karakuzu, M. Sarikanat, Y. Seki, E. Akar, L. Cetin, O.C. Yilmaz, K. Sever, L. Sen, and B.O. Gurses, Improvement of the electromechanical performance of carboxymethylcellulose-based actuators by graphene nanoplatelet loading. *Cellulose* **22**, 3251–3260 (2015).
161. X. Zhang, X. Liu, W. Zheng, and J. Zhu, Regenerated cellulose/graphene nanocomposite films prepared in DMAC/LiCl solution. *Carbohydr. Polym.* **88**, 26–30 (2012).
162. J.-H. Kim, S. Mun, H.-U. Ko, G.-Y. Yun, and J. Kim, Disposable chemical sensors and biosensors made on cellulose paper. *Nanotechnology* **25**, 092001 (2014).
163. G.-H. Kim, S. Ramesh, J.-H. Kim, D. Jung, and H.S. Kim, Cellulose-silica/gold nanomaterials for electronic applications. *J. Nanosci. Nanotechnol.* **14**, 7495–7501 (2014).
164. W.J. Orts, J. Shey, S.H. Imam, G.M. Glenn, M.E. Guttman, and J.-F. Revol, Application of cellulose microfibrils in polymer nanocomposites. *J. Polym. Environ.* **13**, 301–306 (2005).
165. M. Yadav, S. Mun, J. Hyun, and J. Kim, Synthesis and characterization of iron oxide/cellulose nanocomposite film. *Int. J. Biol. Macromol.* **74**, 142–149 (2015).
166. S.K. Mahadeva and J. Kim, Hybrid nanocomposite based on cellulose and tin oxide: Growth, structure, tensile and electrical characteristics. *Sci. Tech. Adv. Mater.* **12**, 055006 (2016).
167. J. Kim, L. Zhai, S. Mun, H.-U. Ko, and Y.-M. Yun, Cellulose nanocrystals, nanofibers, and their composites as renewable smart materials, in *The 22nd International Symposium on Smart Structures and Materials & Nondestructive Evaluation and Health Monitoring*, vol. 9434, pp. 1–6, International Society for Optics and Photonics, Bellingham, WA (2015).
168. P.A. Marques, T. Trindade, and C.P. Neto, Titanium dioxide/cellulose nanocomposites prepared by a controlled hydrolysis method. *Compos. Sci. Technol.* **66**, 1038–1044 (2006).
169. B.-W. Kang, S. Mun, H.-U. Ko, L. Zhai, J.-H. Kim, and J. Kim, Electromechanical behavior of green cellulose-ZnO hybrid nanocomposite. *J. Biobased Mater. Bio.* **8**, 137–142 (2014).
170. M.B. Turner, S.K. Spear, J.D. Holbrey, and R.D. Rogers, Production of bioactive cellulose films reconstituted from ionic liquids. *Biomacromolecules* **5**, 1379–1384 (2004).
171. J. Wu, J. Zhang, H. Zhang, J. He, Q. Ren, and M. Guo, Homogeneous acetylation of cellulose in a new ionic liquid. *Biomacromolecules* **5**, 266–268 (2004).
172. S. Zhu, Y. Wu, Q. Chen, Z. Yu, C. Wang, S. Jin, Y. Ding, and G. Wu, Dissolution of cellulose with ionic liquids and its application: A mini-review. *Green Chem.* **8**, 325–327 (2006).
173. H. Zhang, J. Wu, J. Zhang, and J. He, 1-Allyl-3-methylimidazolium chloride room temperature ionic liquid: A new and powerful nonderivatizing solvent for cellulose. *Macromolecules* **38**, 8272–8277 (2005).
174. S. Barthel and T. Heinze, Acylation and carbanilation of cellulose in ionic liquids. *Green Chem.* **8**, 301–306 (2006).
175. B. Kosan, C. Michels, and F. Meister, Dissolution and forming of cellulose with ionic liquids. *Cellulose* **15**, 59–66 (2008).
176. R.P. Swatloski, S.K. Spear, J.D. Holbrey, and R.D. Rogers, Dissolution of cellose with ionic liquids. *J. Am. Chem. Soc.* **124**, 4974–4975 (2002).

177. S.K. Mahadeva, J. Kim, and C. Jo, Effect of hydrophobic ionic liquid loading on characteristics and electromechanical performance of cellulose. *Int. J. Precis. Eng. Man.* **12**, 47–52 (2011).
178. W. Lu, A.G. Fadeev, B. Qi, E. Smela, B.R. Mattes, J. Ding, G.M. Spinks, J. Mazurkiewicz, D. Zhou, G.G. Wallace, D.R. MacFarlane, S.A. Forsyth, and M. Forsyth, Use of ionic liquids for π-conjugated polymer electrochemical devices. *Science* **297**, 983–987 (2002).
179. S.K. Mahadeva and J. Kim, Nanocoating of ionic liquid and polypyrrole for durable electro-active paper actuators working under ambient conditions. *J. Phys. D Appl. Phys.* **43**, 205502 (2010).
180. L.-J. Zhao, C.-P. Tang, and P. Gong, Correlation of direct piezoelectric effect on EAPap under ambient factors. *Int. J. Autom. Smart Technol.* **7**, 324–329 (2010).
181. S.K. Mahadeva, S. Yun, and J. Kim, Dry electroactive paper actuator based on cellulose/poly (ethylene oxide)—poly (ethylene glycol) microcomposite. *J. Intell. Mater. Syst. Struct.* **20**, 1141–1146 (2009).
182. S.Y. Yang, S.K. Mahadeva, and J. Kim, Remotely powered and controlled EAPap actuator by amplitude modulated microwaves. *Smart Mater. Struct.* **22**, 017001 (2012).
183. J. Kim, S.Y. Yang, G.-Y. Yun, S. Jang, and K. Yun, Cellulose electro-active paper actuator, sensor and beyond, in *The 17th International Symposium on Smart Structures and Materials & Nondestructive Evaluation and Health Monitoring*, vol. 7287, pp. 1–10, International Society for Optics and Photonics, Bellingham, WA (2009).
184. H. Kim, G.Y. Yun, J. Lee, and J.H. Kim, Piezoelectric paper speaker using a regenerated cellulose film, in *The 17th International Symposium on Smart Structures and Materials & Nondestructive Evaluation and Health Monitoring*, vol. 7439, pp. 1–6, International Society for Optics and Photonics, Bellingham, WA (2009).
185. A.G. King, Research advances: DRPs: Let the blood flow; smart cellulose may mean paper airplanes that fly like butterflies; converting biomass directly into electricity. *J. Chem. Educ.* **84**, 10 (2007).
186. D. Hanson, G. Pioggia, Y. Bar-Cohen, and D. De Rossi, Androids: Application of EAP as artificial muscles to entertainment industry, in *Proceedings of EAPAD, SPIE's 8th Annual International Symposium on Smart Structures and Materials* (2001).

